UTRECHT UNIVERSITY
Inorganic Chemistry & Catalysis

MASTER THESIS

The Influence of Chlorine on the Performance of Pt/Al_2O_3/zeolite Y Bifunctional Catalysts

Author:
Renée A. VAN ALST BSc.

Supervisors:
Jogchum OENEMA MSc.

prof. dr. ir. Krijn P. DE JONG
dr. Peter NGENE

January 21, 2018

Abstract

Bifunctional metal-acid catalysts are widely applied in the petrochemical industry for the conversion of various hydrocarbon feedstocks into high quality liquid fuels. In a previous study, Pt/Al_2O_3/Zeolite Y catalysts with a so-called 'nanoscale' intimacy between platinum sites and zeolite acid sites were found to be optimal for the selectivity towards desired isomer products. However, the 'nanoscale' catalyst was prepared with H_2PtCl_6 as metal precursor and it is known that the presence of chlorine results in highly acidic Al_2O_3. Therefore, in this study the influence of chlorine on the catalytic performance of Pt/Al_2O_3 and Pt/Al_2O_3/Zeolite Y bifunctional catalysts with ranging intimacies is investigated.

Via incipient wetness impregnation and strong electrostatic adsorption, zeolite based bifunctional catalysts were prepared with a mili-, micro- and nanoscale intimacy and varying chlorine content. Furthermore a wide variety of Pt/Al_2O_3 references were prepared and analyzed with NH_3-TPD and pyridine-IR in order to examine the influence of chlorine on the surface acidity. In a flowrence 16 parallel fixed bed reactor set-up, the catalytic performance of the bifunctional catalysts and reference samples was examined in the conversion of n-heptane.

The obtained results indicate that chlorine does not have significant effect on the catalytic performance of the zeolite based microscale and nanoscale bifunctional catalysts. Furthermore, observed differences in catalytic performance of the Pt/Al_2O_3 references were, besides the chlorine content, mainly caused by a variety in the average platinum nanoparticle size.

Contents

Chapter 1

Introduction

Catalysis is of essential importance to our modern world and economy and is applied in 85% of all industrial processes. Of all these catalytic processes, 80% is heterogeneous in nature.[1,2] The global petrochemical industry, in which heterogeneous catalysis is widely applied, was estimated to be worth 515 billion USD in 2014 and is expected to increase up to 760 billion USD in 2022 as a result of a growing demand, illustrating both the economical and industrial relevance of petrochemical reforming.[3] In the petrochemical industry, fuels and chemicals are produced out of crude oil, in a sequence of many different catalytic processes. A schematic overview of a typical oil refinery is represented in Figure 1.1.[4]

Crude oil obtained from a well contains a mixture of mostly saturated hydrocarbons over a wide range of chain sizes. The conversion starts with a fractionated distillation in which the crude oil is separated based on boiling point. The heavy (high boiling point) fraction is further separated in a sequential vacuum distillation. Especially the heavier fractions will undergo extensive hydrodesulphurization (HDS) treatments, since they tend to have increased concentrations of sulfur containing hydrocarbons. Environmental regulations have become stricter and define the maximum concentration of sulfur that fuels may contain. The light fractions will undergo at most moderate HDS treatments.[4] The catalytic processes occurring after the two distillations can be considered as 'product upgrading':[4] The distillates are treated in order to obtain high quality products, since the hydrocarbons that are acquired after distillation will either mostly contain a too low octane number to be suitable for gasoline, or will be too long. The chains will undergo subsequent reforming: heavy fractions are cracked either catalytically[5] or processed with hydrogen.[6] In isomerization reactions and reforming processes, the amount of branching and aromaticity of the fractions is increased to obtain the gasoline quality that is required for the market.[1,4]

Gasoline based fuel quality is classified with the research octane number (RON), which is an indication for the amount of branched and aromatic compounds in petrol. A higher octane number indicates a higher quality gasoline fuel, due to better knocking resistance. Fuel will then be less likely to self-ignite in the engine. Historically the RON was set as an empirical value between 0 and 100, in which the properties of n-heptane was set as a RON of '0' and 2,2,4-trimethylpentane (i-octane) was set to '100' since it was most stable.[7] Besides gasoline, there are also other fuels applied, with different quality requirements. Diesel or kerosene for example should mostly contain linear hydrocarbons to ensure proper ignition of the fuels under pressure. This difference in fuel requirements is based on the working mechanism of the engine. Diesel quality is therefore classified with a Cetane Number (CN).[1,4] In Figure 1.2 several hydrocarbons are classified in terms of their RON and CN.

A wide variety of catalysts is applied in the crude oil conversion. Molybdenum

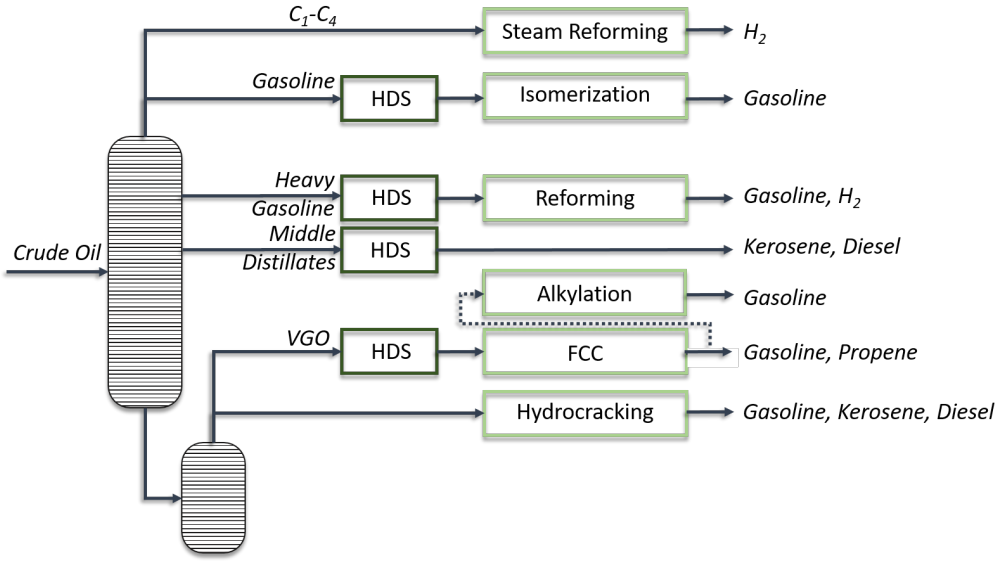

FIGURE 1.1: *Overview of catalytic processes appearing in the crude oil conversion. (Based on)*[4]

	RON	CN
n-hexadecane	-30	100
n-heptane	0	56
n-hexane	25	45
i-octane	100	-
i-butane	102	-
propane	112	-2
methylnaphtalene	-	0

(a)

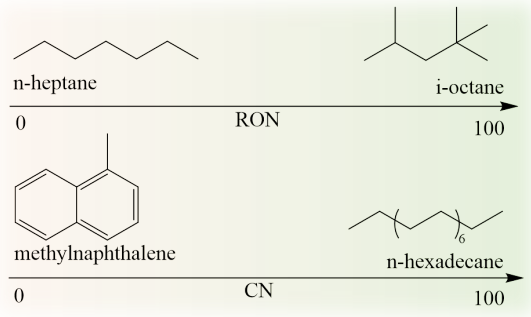

(b)

FIGURE 1.2: *(a): Highlight of RON and CN of some saturated hydrocarbons.*[8] *(b): Schematic depiction of RON and CN scale from '0' to '100'.*

Disulfide (MoS_2) based catalysts are often applied in the HDS treatment. The fluid catalytic cracking process (FCC), the catalytic process performed on the vacuum gas oil (VGO) fraction obtained from the vacuum distillation, is performed by zeolite Y at a temperature around 750 °C. Zeolites are also regularly applied in modern hydrocracking (300-450 °C) and (hydro)isomerization (250-280 °C) processes as active phase and support material for noble metal nanoparticles, usually platinum. Especially for the platinum based catalysts, it is essential that the feedstock contains only very low concentrations of sulfur, while FCC catalysts are less sensitive for sulfur impurities, since this is burnt off in the regenerator.[1,9] The reforming process (460-540 °C),[10] in which the heavy gasoline fractions are upgraded to gasoline, is generally performed by Pt or Pt/Re based catalyst on an acidified γ-alumina support, usually by chlorination.[1]

Hydrocracking, hydroisomerization and reforming processes all occur via a bifunctional mechanism, in which both the metal nanoparticles and catalyst support contribute to product formation.[4] Not only are these processes of vital importance

for the crude oil conversion, they can also be of substantial contribution towards the commercial production of green fuels: Bifunctional catalysts are one of the few systems that can selectively convert long hydrocarbon feedstocks, which could be acquired in a renewable way from biomass.[11] Biomass is currently investigated for the direct production of oil with for example algae,[12] and for the production of syngas, which is applied in the Fischer-Tropsch synthesis.[13] Furthermore, bifunctional catalysts have been investigated for the preparation transportation fuels out of waste plastics, and research has shown that product yield could be tuned towards longer hydrocarbons.[14] Fine tuning of these bifunctional catalysts in terms of activity, selectivity and stability can have tremendous effect on catalyst performance and many research is performed on these systems for obtaining fuel products in high selectivity.[15–17]

This thesis focuses on the catalytic activity, selectivity and stability of platinum based bifunctional catalyst. First theory related to the bifunctional mechanism, side reactions and preparation methods are treated in Chapter 2. On the basis of previously reported research around bifunctional catalyst the scope of this thesis will be outlined and the aim is described in Chapter 3. The thesis will continue with a description of research performed and summarize obtained results in Chapter 5. In the conclusion and outlook, an overview is given of the most important findings and future experiments are proposed.

Chapter 2

Theory

This chapter starts with a general introduction on bifunctional catalysts before the influence of several parameters on the performance of these systems is considered. Next, the bifunctional mechanism for hydrocarbon conversion is described in detail. Also, theory related to the preparation of these catalysts is covered. In a separate section, the effect of chlorine on these systems in terms of catalytic performance and support acidity is described.

2.1 An Introduction on Bifunctional Catalysts

Bifunctional catalysts, as the name indicates, have a two-fold functionality arising from both the nanoparticle metal sites and the surface acid sites of the support material. Noble metals like Pt are known to catalyze dehydrogenation and hydrogenation reactions of hydrocarbons (1). In combination with a support material that contains brønsted acid sites, like a zeolite or a chlorinated alumina, the initial linear feedstock can be converted into isomers (2) and (hydro)cracked products (3).

$$C_nH_{2n+2} \longleftrightarrow C_nH_{2n} + H_2 \quad (1)$$

$$n\text{-}C_nH_{2n} \longleftrightarrow i\text{-}C_nH_{2n} \quad (2)$$

$$C_{l+m}H_{2(l+m)+2} + H_2 \longrightarrow C_lH_{2l+2} + C_mH_{2m+2} \quad (3)$$

Because the alkane feedstock can undergo both isomerization and cracking reactions, depicted in reactions 2 an 3, after the dehydrogenation, the conversion can result in many different products.[15]

First of all the formed alkenes can be isomerized and hydrogenated, forming isoalkanes with the same amount of initial carbon atoms. Secondly, the alkenes can be cracked, followed by hydrogenation. In a bifunctional catalyst, this will be the largest contribution to the product yield. Also, overcracking can occur, which will form gas product. This reaction is undesired, but has a higher contribution at elevated temperatures. Lastly, overcracking of the alkenes can result in blocking of active surface sites, which is termed coke formation. This process will deactivate the catalyst, especially at high temperature regimes. A schematic overview of the possible reactions is depicted in Figure 2.1.

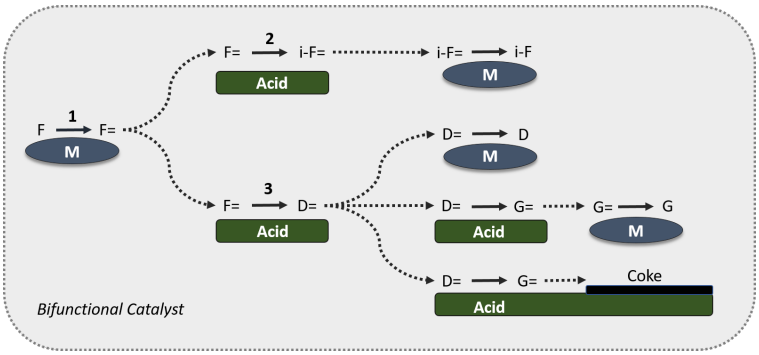

FIGURE 2.1: *Overview of hydrocracking and hydroisomerization of an alkane feedstock (F) over a bifunctional catalyst. Numbers correspond to the depicted reactions. Solid arrows indicate reaction on either metal site (M) or support acid site. Dashed arrows indicate the diffusion of reaction intermediates towards other sites. D = primary cracked product, G = gas product by overcracking. (based on)*[15]

Which of these reactions will mainly occur depends on several parameters. For this reason, bifunctional catalysts have been extensively investigated and are still a topic of current research. Three of the most contributing parameters are described below.

Metal site/Acid site ratio: The ratio between metal sites and acid sites (C_{Pt}/C_a) will influence the activity, selectivity and stability of the catalysts. In a study on this ratio, it was determined that a ratio of $C_{Pt}/C_a \geq 0.17$ was optimal for n-C_{10} transformations: All the acid sites are then provided with alkene reactants, hence the reactions on the acid sites are rate determining. Because the acid sites are constantly fed with new alkenes, the probability of secondary cracking and coke formation is quenched. If the ratio is lower than 0.03, there is an abundance of acid sites compared to metallic sites. In such a scenario, the chance of secondary cracking is increased and deactivation is rapid. The reactions on the metallic sites are then rate determining.[18,19]

Support pore size: The pore size of the support on which the acid sites are located will influence the amount of branching and cracking of the feedstock. If the pores are very small, long branched hydrocarbons will simply not be able to diffuse from the pores and thus will barely form. Cracking is then more likely to occur and the products obtained will mainly consist of short linear hydrocarbons.This limitation can be overcome by using a mesoporous, acidic support material, although in practice these are less active.[17,20,21]

Metal site - Acid site distance: One of the current most extensively studied features of bifunctional catalyst is the distance between metal and acid site.[22–24] The intimacy between metal sites and (brønsted) acid sites influences the product selectivity for hydrocarbon conversion. In early research it was concluded that a minimal distance between these two sides was optimal and that a larger distance would decrease the catalytic activity. When the proximity between the sites is too large, very little catalytic activity is observed, with low selectivity towards isomers. This phenomenon was described with the intimacy criterion.[25] A recent study however has shown that a nanoscale intimacy between metal and acid sites is preferred. In a Pt-Y/Al_2O_3 (closest proximity) catalyst less isomer yield was obtained compared to a Pt-Al_2O_3/Y (nanoscale intimacy) catalyst, contradicting the previous findings of 'the closer the better', as is shown in Figure 2.2.[15]

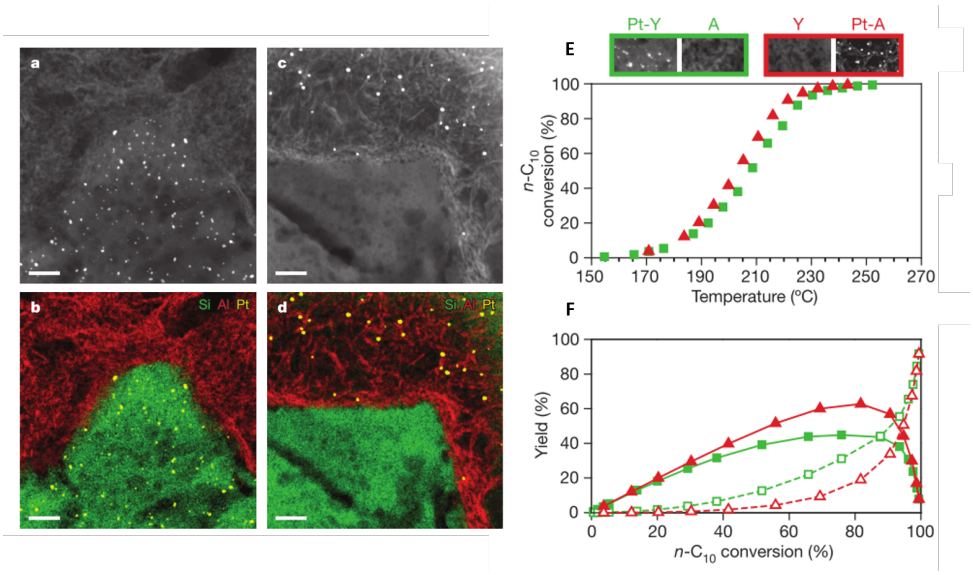

FIGURE 2.2: *HAADF-STEM and EDX results of Pt-Y/Al_2O_3 (closest proximity) (a,b) and Pt-Al_2O_3/Y (nanoscale intimacy) (c,d). e) Catalytic activity of both catalysts in n-C_{10} conversion. f) Isomer yield (closed symbols) and Cracked yield (open symbols) for both catalysts.*[15]

The three parameters considered describe characteristic features of the bifunctional catalysts itself. However, other factors will also influence the activity of the catalyst and should not be ignored. In general heterogeneous catalysts are susceptible for surface impurities, which can block active sites or change electrochemical environment.[26] It is known in the case of bifunctional catalysts that halogens like Cl can acidify alumina and therefore influence product selectivity and amount of branched product formation in hydrocarbon conversion reactions.[27,28] This effect will be discussed in more detail later in Chapter 2. Also particle size effects can play a significant role. When metal particles exhibit a lower surface to volume (S/V) ratio, relatively less catalytically active surface will be exposed, which can alter turn over frequencies (TOF) or influence catalyst deactivation.[1] For these reasons it is of essential importance to compare catalyst samples in a legitimate way. Catalysts should have comparable weight loading, metal particle size and dispersion compared to each other. Also reaction conditions have shown to influence product selectivities and yields in a significant way, so generally those should be comparable as well.

2.1.1 Reaction mechanism and related side reactions

The mechanism of hydroisomerization and hydrocracking over a bifunctional catalyst has been described in detail by Weitkamp.[29] The mechanism consists of several consecutive steps.

First a hydrocarbon molecule is dehydrogenated to an alkene on the metal site. This alkene can then diffuse to the brønsted acid sites of the support where it is protonated, yielding a carbenium intermediate. Due to the instability of a linear carbenium molecule, it is likely to undergo skeletal rearrangements. The overall energy of the molecule is then decreased due to an increase in branching on the positively charged atom. Isomerization of the carbenium ions on the acid sites is considered to be the rate determining steps in these systems.[30,31] There are two types of skeletal rearrangements that can occur. In type A rearrangements, which is considered to be

a fast transformation, the total amount of branching does not increase, but the position of the branch can be altered as a result of alkyl and hydride shifts. In type B rearrangement, which occurs through protonated cyclopropane (PCP) intermediates, the total amount of branching in the molecule increases but this reaction is roughly 5 times slower than type A rearrangements.[18,29] An overview of both rearrangements is given in Figure 2.3a. The molecule can undergo skeletal rearrangements several consecutive times depending on the length of the hydrocarbon. Afterwards, the intermediate can undergo several types of β-scission reactions, which are depicted in Figure 2.3b. Which type of β-scission will occur depends on both the total amount of C-atoms of the molecule 'i' and the amount of present branches. In general, if the charge of the carbenium is transfered from a tertiary or secondary position to a secondary or primary position the reaction will not occur due to product instability, hence the reverse is favorable. Type A β-scissions, which result in a tertiary carbenium ion, are determined to be the fastest. For this kind of β-scission to occur, the hydrocarbon should at least contain 8 carbon atoms and 3 branches. When the molecule contains 7 or more C-atoms, type B_1 and B_2 β-scissions can occur. These yield a tertiary or secondary carbenium ion respectively. Type C β-scissions are very slow, 200 times slower than type B β-scissions,[18] and should not play a significant role in product formation at low temperatures. Type D β-scissions (not shown), yield a highly unstably primary carbenium ion, and are therefore considered forbidden. In order for β-scission to occur, the positive charge of the carbenium must be at a specific place relative to the branches, even though the most stable position for the charge is at the tertiary position. The charge can easily change position on the molecule via hydride shifts. Overall, the position of the positive charge is formulated by Boltzmann statistics, in which the probability of the charge to be at a higher energetic position, like a secondary position, is dependent on the local temperature.[1]

Testing the catalytic performance of bifunctional catalysts with a long hydrocarbon feedstock is preferable since all types of β-scissions can occur.[29] However, the product range will increase as well, which might complicate the analysis. For this reason, the conversion of n-heptane is commonly applied as a model reaction when studying bifunctional catalysts,[19,32] although other feedstocks have been applied as well, like n-decane[18] or n-hexadecane.[23,33,34] Figure 2.4 illustrates the bifunctional mechanism in case of an n-heptane feedstock. Only type B and C β-scissions are taken into consideration. The product distribution mainly consists of 3 groups of products: the i-C7 products (blue), in which type B skeletal rearrangement occurred, but no β-scission has taken place. Primary cracked products (green), in which type B β-scission has taken place after multiple type B rearrangements on carbenium intermediates. The orange product group shows products formed after type C β-scission, which can occur on monobranched carbenium ions. This group consists of linear products. These compounds cannot undergo further transformation via the bifunctional mechanism, since they all contain less than 6 carbon atoms, unless type D scissions are taken into consideration.

Several other mechanisms can contribute to the overall product yield during bifunctional hydrocarbon conversion, depending on mainly the temperature:

- **Classical alkane cracking**
  When the temperature is elevated, (500 °C) classical alkane cracking can occur on the support acid sites only, which is termed monofunctional acidic cracking. In this mechanism a hydride transfer occurs between an alkane and carbenium

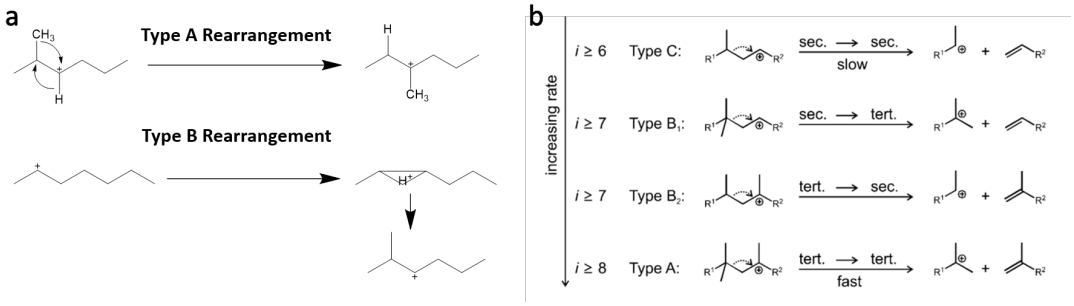

FIGURE 2.3: *a) Representation of both forms of rearrangements that can occur on a carbenium ion. Type A rearrangement happens via alkyl and hydride shifts, Type B rearrangements occur via PCP mechanism. b) Overview of the different types of β-scissions that can occur on a bifunctional catalyst as function of total number of carbon atoms 'i'.*[29]

ion, forming a more stable carbenium ion. The mechanism however does not explain the formation of the prerequisite carbenium ion.[35]

- **Haag-Dessau cracking**
  Non classical cracking can occur when the temperature is reasonably high (350-550 °C),[35] which is termed Haag-Dessau cracking.[29] In this mechanism, an alkane is protonated to form a carbonium ion, which contains a 5 coordinated carbon atom. This protonation can only be done on superacidic sites, for example on a zeolite. Cracking of these species has shown to lead to mostly small linear hydrocarbons like methane and ethane, hence it shows a significantly different product profile than bifunctional conversions. A carbonium intermediate is much more unstable than a carbenium intermediate and will only form at elevated temperatures, since alkenes formed after dehydrogenation are more prone to be protonated than an already saturated hydrocarbon.[35]

- **Metal Cracking**
  Cracking can also occur on the metal sites only, which is described by hydrogenolysis, also termed metal cracking. In general metal cracking will result in linear products.[29] In a study by Carter *et al.*, it was shown that unsupported samples of different noble metals show ranging metal cracking product distributions which was associated with the amount of d-character of the metal. Metals exhibiting a high amount of d-character, like ruthenium or rhenium, showed high selectivity towards terminal C-C bond breaking of n-heptane, resulting in n-hexane product. However, Pt, exhibiting relatively little d-character, showed to have a more non selective metal cracking profile including all linear hydrocarbons up to C6, compared to more d-character pronounced metals. Furthermore, besides metal cracking, pure Pt samples showed to have a significant yield of isomers, even at 325 °C.[36]

- **Hydropyrolysis**
  The last form of cracking that can occur is thermal non-catalytic cracking, also termed hydropyrolysis. This mechanism includes free radical intermediates.[35] At high temperatures (500-600 °C) and significant pressures of hydrogen this cracking can contribute considerably to the product distribution.[29]

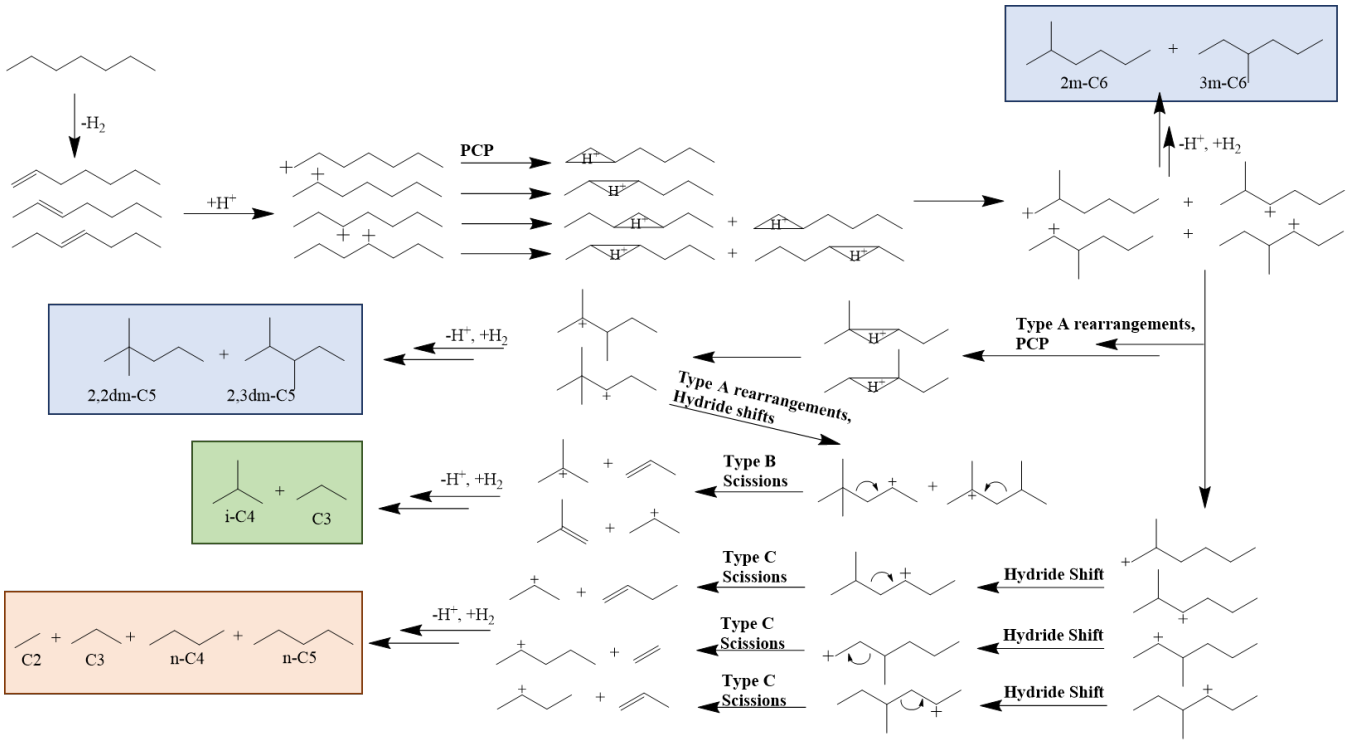

FIGURE 2.4: *Bifunctional mechanism for n-heptane conversion in hydrogen atmosphere. i-C7 yield: blue, primary cracking yield (green), linear yield (orange).*

2.1.2 Preparation methods

For the preparation of heterogeneous catalysts in general, many different procedures have been reported ranging from impregnations to colloidal synthesis based protocols in model catalysts.[1] For bifunctional catalysts preparation, the synthesis is mostly based on (Incipient Wetness) Impregnation (IWI) techniques, Strong Electrostatic Adsorption (SEA) or Ion Exchange (IE). Those procedures will be covered in detail.

Incipient Wetness Impregnation

Incipient Wetness Impregnation is a relatively simple but effective method for preparing heterogeneous catalysts. It is commonly applied in the preparation of heterogeneous catalysts for industrial purposes. The first step is the drying of support material (under vacuum), at elevated temperatures to remove adsorbed water from the pores. Then, a solution of metal precursor is added with the same volume as the total pore volume of the support, to ensure complete pore filling. Doing so will enhance the homogeneity in dispersion of the metal precursor. The third step is to dry the sample in order to remove the solvent of the precursor solution. The last step is a heat treatment to convert the adsorbed metal complexes into metal(oxide) nanoparticles. The obtained metal particle size is dependent on many parameters, including reduction temperature, applied precursor, support material, solvent and drying procedure.[37] Furthermore, the average particle size can be increased by applying certain temperature profiles or gas atmospheres in an aftertreatment.[38–40] Pt based catalysts can be easily prepared with IWI and this has been performed in other studies on a variety of supports like alumina,[28,41] silica[40] or zeolites.[16,42]

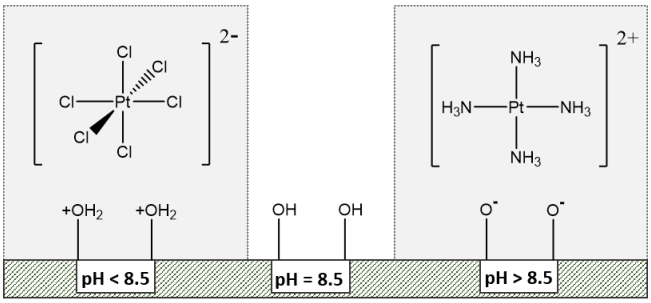

FIGURE 2.5: *Process of SEA for an alumina support at pH < 8.5, at which a negatively charged Pt precursor can be used like hexachloroplatinic acid (CPA), and at pH > 8.5, at which a positively charged Pt precursor can be used like platina-tetraammine (PTA).*

Strong Electrostatic Adsorption/Ion Exchange

In a SEA procedure, a solution of platinum precursor is added to a suspension containing excess of demineralized water with respect to support material. Generally, the pH of this suspension is adjusted to maximize the surface charge of the support, thereby enabling maximum adsorption of oppositely charged metal precursor.
A γ-alumina surface has a point of zero charge (PZC) of pH$\approx$ 8.5,[43] indicating that the surface will have no net charge at this pH. When the pH of the solution is altered, the hydroxyl surface groups of the support will become either positively charged (below PZC) or negatively charged (above PZC). When a metal precursor is added with opposite charge compared to the surface groups, electrostatic adsorption will take place. The mechanism has been described in detail by Spieker *et al.*[43] and Brunelle[44] and is schematically depicted in Figure 2.5. A SEA procedure can also be applied for preparation of Pt/Zeolite catalysts.[15,24,45] Zeolites are very acidic supports compared to alumina or silica and have a PZC value of pH$\approx$ 2-4.[44]

Several parameters have to be taken into account during the procedure.

1. **Support Solubility**: When the pH of the suspension is too high or low, the support might dissolve. This results in loss of yield but also in a higher metal weight loading than calculated if the desired precursor loading was lower than

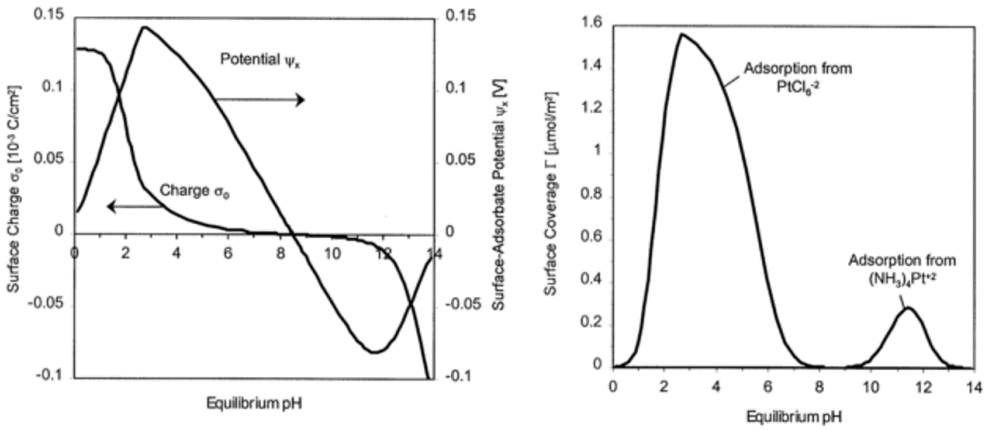

FIGURE 2.6: *Surface charge (left) and corresponding ion uptake (right) of an alumina support as function of solvent pH.*[43]

the maximum obtainable support surface coverage. In case of γ-alumina, at a pH lower than 3, the support will already partly dissolve.[43]

2. **Surface potential**: As a result of pH increase or decrease, the surface will build an electrostatic potential. The surface charge of alumina as function of pH is depicted in Figure 2.6. At low and high pH, besides the fact that the potential is either positive or negative, the alumina support shows a significantly different absolute value, making ion adsorption in a low pH range (large potential) more effective than ion adsorption at a high pH (small potential). This is also seen in the ion uptake.[43]

3. **Metal precursor size**: The maximum amount of metal precursor loading on a support is different when differently sized precursors are used. If a bulky precursor is applied, less of these complexes will fit on the surface, decreasing the maximum obtainable loading. This effect should be taken into consideration when catalysts prepared with different precursors should have equal weight loading. For example, when a 1% weight loading of Pt on γ-alumina is desired, this can be easily achieved with the small CPA precursor, but is challenging with a bulky PTA precursor as depicted in Figure 2.6.[43]

4. **Ionic strength**: When the pH of the solution is too extreme (either way) the metal precursor uptake will diminish. This is caused by a high ionic strength, which counteracts the surface charge, thereby quenching precursor adsorption. Besides pH, another factor that influences the ionic strength is the concentration of counterions as a result of pH adjustment in the procedure. Not only can these counterions compete with the metal precursor, they will also enhance ionic strength at high concentrations.[43]

When application of SEA is compared to an IWI procedure, one of the main advantages is the possibility to selectively deposit a metal precursor on a mixture of supports due to the surface potential, by tuning the pH of the solution and applying an appropriately charged metal precursor. An IWI technique is not selective. However, SEA is not optimal when high weight loadings are desired, because the uptake is always dependent on the maximum possible surface coverage of the precursor. In such a scenario, IWI is easier to apply, especially since impregnation techniques can be repeated to obtain weight loadings that can exceed the maximum support surface coverage.[26]

2.1.3 Alteration of the intimacy

Based on the previously described methods, the preparation of bifunctional catalysts with varying intimacies has been reported in literature.[15,23,24] The platinum nanoparticles are supported on a non-acidic support material like γ-alumina. This material is then mixed with an acidic material like zeolite Y to form bifunctional catalyst. The alumina binder, exhibiting less surface acidity compared to zeolites, is considered to be inactive in the bifunctional mechanism at reasonable low temperatures (200 - 350 $^{\circ}$C). Several degrees of intimacies, depicted in Figure 2.7, are described.

Millimeter intimacy
Bifunctional catalysts with a millimeter scale metal-acid distance can be obtained in different ways, but the platinum metal nanoparticles are always attached to a non-acidic binder material as the metal component of the bifunctional catalyst. The metal component is then loaded into a fixed bed reactor, in which it is layered with

an acidic component and separated by inert layers.[24] Another way to achieve a millimeter scale separation, is to crush and sieve the Pt/Al_2O_3 fraction to grains and then mixing this powder with a zeolite powder of the same grain size, creating a physical mixture.[23] In the preparation of a millimeter scale intimacy, the preparation of Pt/Al_2O_3 is performed in absence of zeolite material, so it can be obtained via both SEA or IWI, depending on the desired weight loading.

Microscale intimacy
A microscale intimacy can be obtained easily after Pt/Al_2O_3 is prepared.[23] By mixing and crushing the metal component with the acidic component in a 1:1 weight ratio, the intimacy of the sample is increased compared to a conventional physical mixture. It is also possible to crush and sieve the metal and acid component separately to a smaller grain size in order to increase intimacy, although the overall intimacy is then lower compared to when they are crushed together.

Nanoscale intimacy
The preparation method for a nanoscale intimacy is described in detail by Zečević *et al.*[15] In this method, platinum nanoparticles are selectively deposited on a composite mixture containing both alumina binder and zeolite material in a 1:1 weight ratio. This is selectively done via SEA, and can therefore not be performed with IWI. Although the paper used a readily available composite for the synthesis, it can also be prepared by mixing alumina binder and zeolite together to a paste, which is described in the methods in Chapter 4.
In another study, a nanoscale intimacy was acquired by selective deposition of platinum on alumina domains of a Si rich Al/Si support. The obtained platinum particles were roughly 15 nm big.[24]

Closest proximity
A bifunctional catalyst with closest proximity can be considered as platinum directly deposited on the acidic support material. These catalysts are applied in industry, in crude oil conversion. Preparation of such a system can be easily performed via either IWI[46] or SEA.[15]

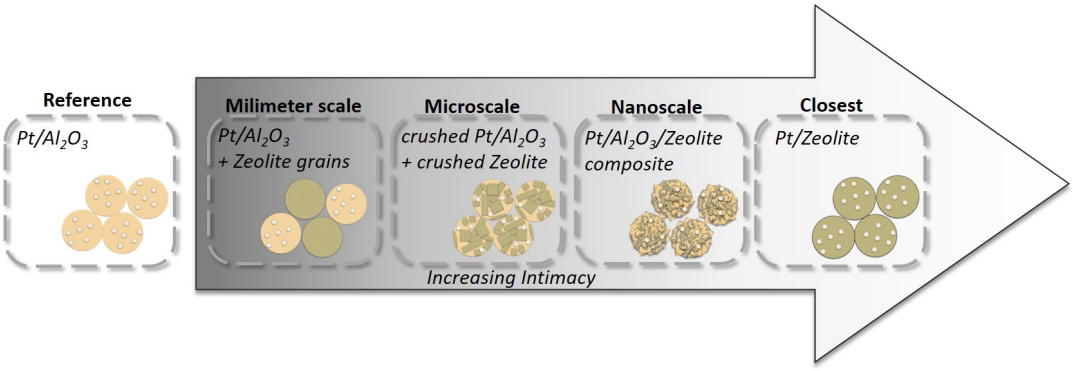

FIGURE 2.7: *Schematic representation of zeolite based bifunctional catalysts with different intimacies ranging from a millimeter scale to a closest proximity, with pure Pt/Al_2O_3 as a reference.*

2.2 Chlorine: addition and influence on catalytic performance

It has been known for a long time that chlorine can have both promoting and poisoning effects on heterogeneous catalysts in general. In the catalytic performance of reforming catalyst and bifunctional systems, the enhanced surface acidity caused by the chlorine content can contribute to certain product selectivities an even influence catalyst stability. Reported analysis on the enhanced surface acidity, preferred chlorine locations and the effect on the catalytic performance is covered.

2.2.1 Surface Acidity

Chlorinated alumina is applied as support for reforming catalysts, to enable isomerization to occur on the acidic sites. When chlorine is present on the surface, its electron withdrawing effect can enhance the brønsted acidity of a proximate hydroxyl group. Often, alumina is chlorinated in a stream of HCl or Cl_2.[31] This method will break Al-O bonds from either surface Al-OH bonds or internal framework Al-O-Al bonds. Eventually, this method will transform Al_2O_3 to $AlCl_3$. A more mild introduction of chlorine to alumina can be done by impregnating the support with an NH_4Cl solution, which is also performed in some studies.[27,47] This technique is considered to only replace surface OH groups and leave the internal structure intact. Figure 2.8 schematically illustrates the effect of HCl and NH_4Cl treatment on an alumina surface. The challenge in applying chlorine to enhance support acidity is its instability on the surface, resulting in loss of surface acidity overtime during reaction. For this reason, chlorine is continuously added to reforming catalyst in industry, mostly by gas or a chlorine containing hydrocarbon feedstock.[31] Although alumina is prone to loose chlorine content overtime, a complete removal of chlorine, for the sake of fundamental research, is challenging. Even at very high temperature aftertreatments it has not been successful to completely remove chlorine.[48]

Support surface acidity can be analyzed by a variety of techniques, but they are generally based on basic probe molecules. These probes will attach to the acid sites and their bonding strength is dependent on the surface acid strength. The surface acidity can arise from both brønsted and lewis acidity. A brønsted acid site is a proton donor, of which an example was shown in Figure 2.8. A lewis acid site is an electron pair acceptor.[49] Two widely reported surface acidity analysis techniques will be briefly explained.

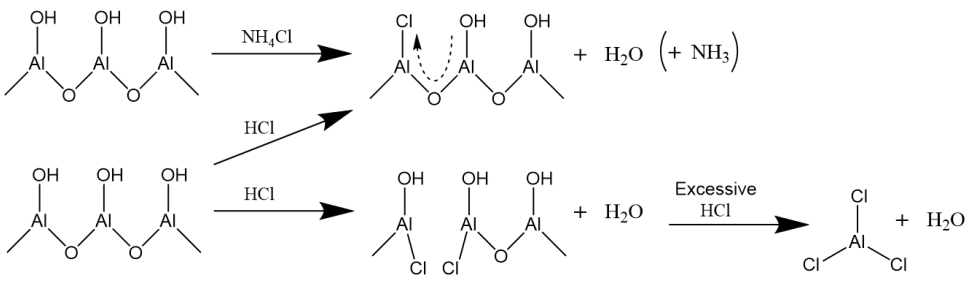

FIGURE 2.8: *Effect of NH_4Cl treatment (top) and HCl treatment (bottom) on an Al_2O_3 surface. NH_4Cl mainly replaces surface OH groups, resulting in increased brønsted acidity due to electron withdrawing properties (dashed arrow). HCl treatment also results in Al-O-Al bond breaking, eventually forming $AlCl_3$.*

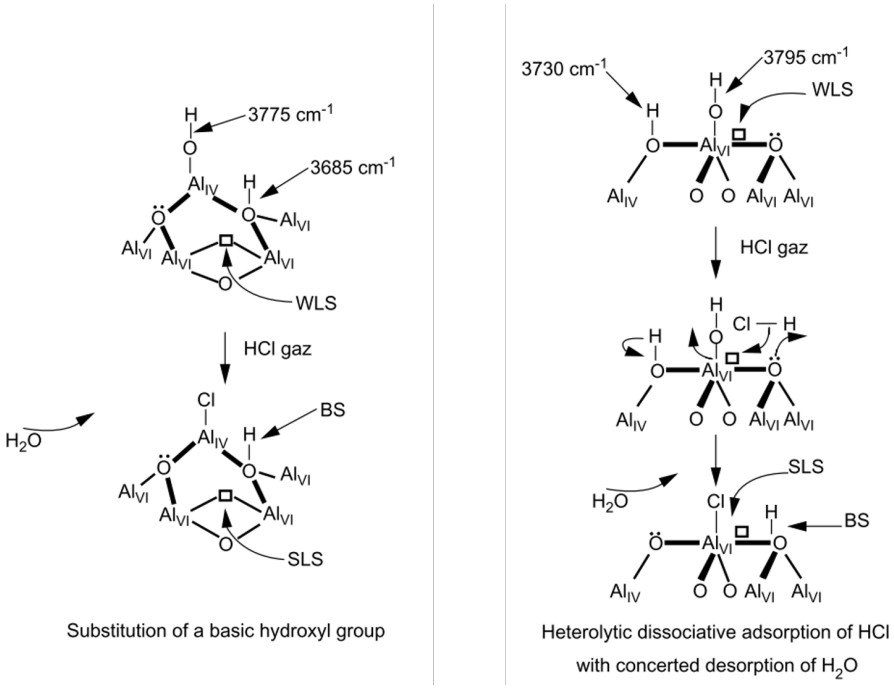

FIGURE 2.9: *The two derived chlorine locations originating from HCl treatment determined via IR and NMR studies on an 110 alumina surface in the spinel C(left) and D(right) layer. WLS = weak lewis site, SLS = strong Lewis site, BS = brønsted acid site.*[50]

In a bulk method, the surface acidity can be measured via ammonia-TPD. In such an experiment, ammonia, being slightly basic in nature, is adsorbed on a heterogeneous catalyst in several pulses. Depending on the acid site strength, ammonia will be more strongly bound to the surface. For a γ-alumina support, a rough distinction can be made between weak and strong acidic sites, on which desorption takes place around 250 and 320-340 °C respectively.[15] Ammonia-TPD has been applied for analysis of Pt/Al_2O_3 surface acidity in other studies.[28,51]

Surface acidity can also be analyzed with probe molecule based IR-spectroscopy. Several probe molecules have been applied, under which also ammonia. The research showed that a distinction could be made between lewis sites (1542 cm^{-1}) and brønsted acid sites (1425 cm^{-1}).[52] However, the chlorine treated catalyst did not show any lewis acidity bands, which was also observed in a different study.[53] Another probe molecule that is widely applied is pyridine. In a pyridine-(FT)IR study, information on both acid site strength and different surface sites can be obtained. Several bands can be expected: Py-LAS(octa) at 1594 cm^{-1}, Py-LAS(tetra/octa): 1615 cm^{-1}, Py-LAS(tetra) at 1623 cm^{-1} and Py-BAS at 1637 cm^{-1}. Chlorine increases both the lewis acidity and brønsted acidity of an alumina support by depleting the surface from electrons and weakening O-H bonds respectively. One thing to keep in mind however is that, in case of Pt/Al_2O_3, measured surface acidity is also dependent on platinum particle size. Platinum particles smaller than 1.5 nm are basic in nature and could therefore slightly compensate for the surface acidity. Since these particles grow as a result of NH_4Cl-impregnation, this basicity is decreased because the electron density is then more restricted to the Pt band structure.[54] An observed increase in surface acidity is then not only caused by just Cl content. In other research, pyridine-IR is used as a method to estimate the amount of acid sites in the bifunctional catalysts.[19]

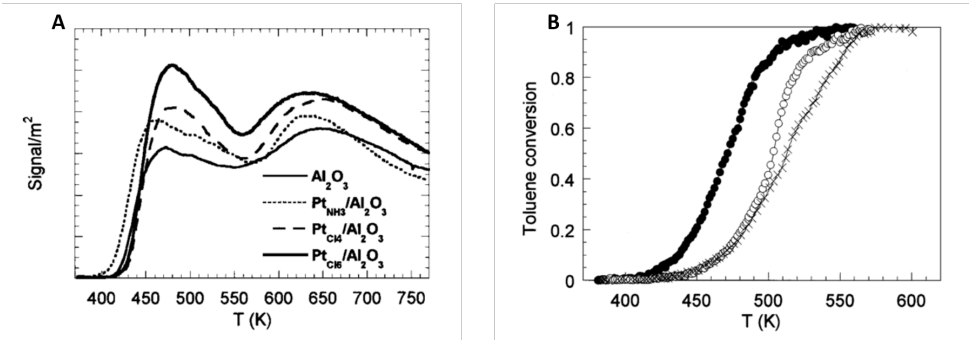

FIGURE 2.10: *A) NH_3-TPD results of Pt/Al_2O_3 prepared with $Pt(NH_3)_4)(OH)_2$, $(NH_4)_2PtCl_4$ and $(NH_4)_2PtCl_6$. B) Catalytic activity of Pt/Al_2O_3 prepared with $Pt(NH_3)_4)(OH)_2$ (black dots), $(NH_4)_2PtCl_4$ precursor (open dots) and $(NH_4)_2PtCl_6$ precursor (crosses).*[27]

The exact location of chlorine on an alumina surface has been extensively studied, and different sites have been proposed.[27,50,55] Digne *et al.* were able to obtain mechanistic insight on the adsorption of chlorine on an alumina surface in combination with DFT calculations. The study showed that competition exists between chlorine and water molecules on the surface.[55] Furthermore, Guillaume and coworkers were able to predict adsorption locations of chlorine atoms on an alumina surface via pyridine-IR measurements combined with NMR studies, in the case of HCl treatment. They showed these sites based on the 110 surface of γ-alumina, which is known to be most common.[56] A highlight of this study is shown in Figure 2.9.

2.2.2 Catalytic performance of Cl doped bifunctional catalysts

The effect of chlorine on Pt/Al_2O_3 or related materials has been widely investigated. Many reports can be found on the activity,[27,28,57,58] selectivity,[58,59] and stability[27,41] of these chlorine impregnated systems. Also studies covering the effect of chlorine on other alumina supported metals can be found.[47,60] Paulis *et al.* studied several Pt/Al_2O_3 catalysts in the complete oxidation of toluene. It was demonstrated that when Pt/Al_2O_3 was prepared with a more chlorine containing precursor, the support acidity changed significantly. Furthermore, the samples showed very different activities, as is highlighted in Figure 2.10.

Guillaume *et al.* studied the effect of the Pt/Al_2O_3 surface acidity on the catalytic performance in the conversion of n-heptane. They observed that the addition of chlorine to the catalysts, via a H_2O-HCl-air stream resulted in an increase of strong brønsted and lewis acid sites, at the cost of weak lewis acid sites. The conversion of n-heptane was performed on a catalyst series with chlorine content ranging from 0 to 1.4 wt.% Cl. The data indicated that an increase in chlorine content resulted in a decrease of i-C7 yield and cyclic products and an increase in primary cracked products. Catalysts containing more than 0.7 wt.% Cl had overlapping product distributions. Based on pyridine-IR results, MAS-NMR and the catalytic tests it was proposed that the conversion of n-heptane was utilizing two different acid sites: the strong brønsted acid sites would enable isomerization, and the strong lewis acid sites would enable cracking to occur.[50]

Chapter 3

Research Objectives

The use of $PtCl_6^{2-}$ is required for the synthesis of nanoscale intimate bifunctional catalysts, which in a previous study showed to have more ideal hydrocracking behavior than a catalyst with a closest metal-acid intimacy prepared with $Pt(NH_3)_4^{2+}$. The 'nanoscale' catalysts product distribution contained an enhanced yield of isomer products and lower yield of cracking products compared to the closest proximity catalyst as was shown in Figure 2.2.[15] However, other research has shown that (residual) chlorine content can influence the catalytic behavior of Pt/Al_2O_3 as a result of an increased surface acidity.[50] A quantitative analysis on the influence of Cl on the catalytic behavior of zeolite based bifunctional catalysts, partly consisting of Pt/Al_2O_3, has not been performed.

To exclude the contribution of residual chlorine on especially the bifunctional catalysts with a nanoscale intimacy, but also on the other intimacies, a study on this effect is of essential importance, in order to confirm if the reported enhanced isomer selectivity is indeed caused by the nanoscale metal-acid distance.

To gain insight in this matter, this study consists of two parts:

- **PART I: Preparation and analysis of Pt/Al_2O_3**
  As reference catalysts, Pt/Al_2O_3 samples will be prepared. This is done with both chlorine free and chlorine containing platinum precursor and can be additionally impregnated with NH_4Cl, to obtain a range in chlorine content between 0 and 2 wt.% Cl.[47] The series of prepared references will be analyzed in terms of their surface acidity and catalytic performance, to examine the effect of chlorine content.
  The aim of Part I is to prepare all Pt/Al_2O_3 with 1 wt.% Pt loading and equal nanoparticle size around 1 nm, to enable a proper comparison.

- **PART II: Preparation and analysis of $Pt/Al_2O_3/Y$**
  The prepared Pt/Al_2O_3 samples are then applied in the preparation of millimeter scale and micrometer scale zeolite based bifunctional scale, which were shown in Figure 2.7. Next, bifunctional catalysts with a nanoscale intimacy will be prepared following the procedure of Zečević *et al.*[15] The catalytic performance of all samples is examined in the conversion of n-heptane.
  The aim of part II is to elucidate the contribution of chlorine on the catalytic performance of the zeolite based bifunctional catalysts with ranging intimacies.

Chapter 4

Experimental

This chapter describes the preparation methods and analysis procedures applied in this study. In Section 4.2, the synthesis procedures are covered and in Section 4.3 the applied analysis techniques are described.

4.1 Chemicals

The table summarized the used chemicals and corresponding suppliers. All the water applied in the synthesis procedures has been filtered with a Direct-Q water purification system (Mili-Q).

Name	Supplier
Chloroplatinic acid hexahydrate (CPA.6H_2O), (99%)	Sigma Aldrich
Chloroplatinic acid hydrate (CPA.xH_2O), (99.9%)	Sigma Aldrich
Tetraammineplatinum(II) nitrate (PTA), (>99.9%)	Sigma Aldrich
Ammonium chloride (99.5%)	Acros
Hydrogen chloride (fuming)	Merck
Acetic Acid (glacial)	Merck
n-Heptane (99%)	Acros
alumina precursor (Boehmite 70%, HMPA)	Shell Technology
alumina precursor (Pural SB), (>99.9%)	Sasol
γ-alumina (Puralox SCCa-2/500), (>99.9%)	Sasol
Silica (Aerosil 380)	Degussa
Zeolite Y (CBV760)	Zeolyst

4.2 Sample Preparation

The reference catalysts have been acquired via IWI and SEA. The nanoscale intimate catalysts have been prepared via SEA.

4.2.1 Reference Samples

Pt/Al_2O_3

Incipient wetness impregnation
In an incipient wetness method, a 100 mL round bottom flask containing 1.00 g Puralox SCCa-2/500 and a stirring bar was dried under vacuum, while heated (moderate stirring) for 90 minutes. The flask is retrieved from the vacuum while maintaining the vacuum inside and the support material is stirred on a stirring plate at moderate speed. 0.45 mL metal precursor solution in mili-Q, containing either 27 mg CPA.xH_2O or 20 mg PTA, is added dropwise to the dried support material in

ca. 5 minutes. The material is stirred for an additional 1.5 hour before it is collected in a crystallizing disk and dried in a 120 °C stagnant air oven overnight. Prior to reduction the material is pelletized and sieved to 75 <x <150 μm using a hydraulic press and a stainless steel press tool. Sieved IWI samples are reduced in a flow of H_2 (100 ml/min/g sample) at 600 °C for 3 hours with a ramp of 5 °C per minute to obtain highly dispersed Pt nanoparticles.

In order to grow reference samples to a larger average Pt nanoparticle size, some Pt/Al_2O_3 samples have been additionally aftertreated at 600 °C for 1 hour in a flow of 1 vol.% O_2 in N_2. These will be called Pt/Al_2O_3-g. In Appendix 9.1, a schematic overview of the reduction and growth procedure treatments is given.

When preparing smaller or larger amounts of catalysts, the quantities are adjusted accordingly.

Strong electrostatic adsorption

In a strong electrostatic adsorption method, 0.50 g γ-alumina, prepared from a 70% Boehmite precursor by calcining the material at 550 °C for 2 hours in a stagnant air oven (5 °C/min), is added to 600 mL mili-Q and stirred at 500 rpm, the pH = 6.5. Depending on the metal precursor the procedure is as following:

- **Chloroplatinic acid hexahydrate:**
  The pH is lowered to pH = 2.6 with a 1M HCl solution and the mixture is stirred for 1 hour. The pH is adjusted if needed. 45 mL metal precursor solution containing 28.9 mg $CPA.6H_2O$ is prepared.

- **Tetrammineplatinum nitrate:**
  The pH is raised to pH = 11 with a concentrated NH_3 solution. The pH is adjusted if needed. 45 mL metal precursor solution containing 20.3 mg PTA is prepared.

The metal precursor solution is added dropwise in ca. 15 minutes to the mixture and it is left to stir for an additional 3 hours. The solid material is collected with a vacuum filtration and dried in a crystallizing dish overnight in a 120 °C stagnant air oven. The samples follow the same reduction protocol as described in the IWI method. Variations on this procedure have been tested in the synthesis of Pt/Al_2O_3. For example, different bases have been applied to raise the pH. Obtained results on those variations are summarized in Chapter 5.1 and Appendix 9.2.

Addition of Chlorine

Chlorine is introduced to the samples via IWI following the same procedure as in preparation of Pt/Al_2O_3 catalysts. For this, 0.5 g as prepared Pt/Al_2O_3 is added to a 100 mL round bottom flask and dried in vacuum for 1.5 hours while moderately stirring. As an impregnation solution, extra pure NH_4Cl, appropriate for desired weight loading of Cl in the sample, is dissolved in 5 mL MQ in a measuring flask and homogenized. After drying, the catalyst is retrieved from the vacuum, while maintaining the vacuum inside the flask, and stirred at moderate speed. 0.225 mL prepared solution is added dropwise in ca. 5 minutes. The material is left stirring for 1.5 hours, collected and dried in a 120 °C stagnant air oven overnight. In total, samples have been impregnated with up to 15 wt.% Cl. To achieve this, samples starting from 9 wt.% were double impregnated due to solubility of the NH_4Cl in Mili-Q, by repeating the procedure. Prior to the aftertreatment, the material is pelletized and sieved to 75<x <150 μm using a hydraulic press and a stainless steel press

tool. Sieved samples are aftertreated at 600 °C for 3 hours in H_2 flow (5 °C/min). The temperature profile is described in Appendix 9.1. The ammonia is assumed to desorb from the catalysts during this aftertreatment.
The chlorine impregnated reference catalysts are also applied in the preparation of millimeter scale and microscale intimate bifunctional catalysts.

Pt/SiO_2

Platinum deposited on a silica support is prepared following the same IWI procedure as for Pt/Al_2O_3. However, 0.73 mL metal precursor solution in mili-Q, containing 44 mg PTA is then added to 1.00 g Aerosil 380.

4.2.2 Bifunctional Catalysts

Millimeter scale: Pt/Al_2O_3/Zeolite Y physical mixtures

The physical mixtures (pm), Pt/Al_2O_3/Y-pm, are prepared by mixing a sieved CBV760 zeolite Y powder with an as prepared, sieved Pt/Al_2O_3 powder to obtain a millimeter scale intimacy between acidic zeolite and metallic Pt function. In this study, only sieving fractions of 75<x <150 μm have been applied in the preparation of millimeter scale bifunctional catalysts.

Microscale: Pt/Al_2O_3/Zeolite Y intimate physical mixtures

The intimate physical mixtures (ipm), Pt/Al_2O_3/Y-ipm are obtained by pelleting, crushing and sieving the as prepared Pt/Al_2O_3 powder and CBV760 in a 1:1 wt. ratio, until a homogeneous light gray mixture is obtained. This powder is then sieved to 75<x <150 μm.

Nanoscale: Pt/Al_2O_3/Zeolite Y composites

The Pt/Al_2O_3/Y-comp samples are obtained by first preparing an Al_2O_3/Zeolite Y composite material and then selectively depositing Pt on the alumina phase:

- **Composite preparation:**
  To a crystallizing dish 20 mL Mili-Q and 400 μL acetic acid are added. 10.0 g Pural SB Boehmite is added and mixed with a mortar until a paste is acquired. 10.0 g CBV760 is added and mixed. Mili-Q is added in portions of $0.5 - 1.0$ mL to aid in the stirring until a homogeneous thick paste is acquired with no visible dry powder. The material is dried in a 120 °C oven overnight.
  The composite is calcined in stagnant air at 550 °C for 2 hours with a ramp of 5.8 °C/min. Afterwards, the obtained composite is sieved to a 212 <x <500 μm fraction.

- **Deposition of Pt:**[15]
  Pt is selectively deposited on the alumina by means of SEA. For this, 1.00 g composite material is added to 600 mL Mili-Q and stirred at 500 rpm. The pH is adjusted to pH = 2.6 with a 1M HCl solution and the suspension is stirred for 1 hour to equilibrate, in which the pH is readjusted if needed.
  A precursor solution containing 14.7 mg CPA(Hydrate) in 50 mL Mili-Q is added to a droplet funnel and added dropwise to the suspension in ca. 15 minutes, in which the pH increases from pH = 2.6 to pH = 2.7. After 3 additional hours of stirring the pH = 2.8. The solid material is collected via vacuum

filtration and dried in a 120 °C stagnant air oven overnight. The composites are reduced following the same procedure as the Pt/Al_2O_3 catalyst.

- **Addition of Chlorine:**
  To the nanoscale intimate bifunctional samples, chlorine is added according to the same procedure as described for the reference catalysts. However, 0.36 mL of prepared NH_4Cl solution, containing the appropriate amount of Cl for desired Cl weight loading, is then added per gram catalyst. In case of the nanoscale intimate samples, the NH_4Cl is added to the zeolite containing composite, rather than to the Pt/Al_2O_3 component as in the microscale and millimeter scale catalysts.

4.3 Analysis

The prepared catalysts are characterized with (high angle annular dark-field scanning) transmission electron microscopy (HAADF-STEM, TEM) and energy dispersive x-ray spectroscopy (EDX)-mapping to determine the platinum nanoparticle size, distribution and location. The weight loading of both Pt and Cl is determined with inductive coupled plasma optical emission spectrometry (ICP-OES). Ammonia temperature programmed desorption (NH_3-TPD) and Pyridine infrared spectroscopy (Pyridine-IR) desorption experiments have been applied to analyze the catalyst surface acidity. Additional thermogravimetric analysis mass spectroscopy (TGA-MS) experiments have been performed to determine Cl desorption temperatures. The samples are also tested in hydrocarbon conversion in terms of catalytic activity, selectivity and stability. The applied techniques and procedure for corresponding analysis are shortly described.

4.3.1 TEM/HAADF-STEM/EDX

Analysis was performed on a FEI Talos^{TM} F200X device. The nanoscale intimate samples are microtomed prior to measurements. Analysis of the data is performed via iTEM software package, for which the size of at least 300 nanoparticles was counted if achievable.

4.3.2 ICP-OES

Measurements are performed by Kolbe Mikroanalytisches Laboratorium in Mülheim an der Ruhr, Germany. Prior to the analysis, the sent samples were dried at 120 °C, 5 mbar.

4.3.3 TGA-MS

Samples were measured with a PerkinElmer Pyris I TGA device, in a temperature program up to 600 °C. For the analysis, m/z ratios corresponding to related chemicals were followed, which are summarized in Table 4.1, including their expected relative intensities.

Compound	m/z ratios
H_2O	18 (100), 17 (20)
HCl	38 (30), 36 (100), 35 (18)
Cl_2	*72 (65)*, 70 (100), 37 (30), 35 (82)
NH_3	17 (100), 16 (80)
NH_4Cl	38 (35), 36 (100), 35 (13), 17 (65), 16 (45)

TABLE 4.1: *Overview of measurable m/z ratios per chemical. The characteristic intensities are depicted in brackets per m/z value. For Cl_2, only the m/z = 70 has been evaluated since this value was not overlapping with other m/z ratios.*

4.3.4 NH_3-TPD

For the NH_3-TPD analysis, 100 mg of sample was loaded between layers of quartz wool in a quartz reactor tube. The desorption of ammonia is measured up to 550 °C with an Autochem II 2920 automated characterization system, coupled to a Thermal Conductivity detector (TCD). For the analysis and quantification of the data, Origin9.1 is applied. Quantification of the TPD plots has been performed by first plotting the TCD signal as function of time and then deconvoluting the spectra to obtain the area corresponding to the strong acid site signal (maximum roughly at 340 °C). Desorption of NH_3 from these strong acid sites is then calculated via formula 4.1. For the calculation of the total amount of NH_3-desorption, the area corresponding to complete deconvoluted spectrum is applied in the formula.

$$D_{NH3} = 0.01AdM * \frac{F}{m} \tag{4.1}$$

- D_{NH3} = total amount of desorption from strong acid sites (mol/g catalyst)
- A = area corresponding to strong acid site signal (unitless)
- d = density of ammonia (0.769^{-3} g NH_3/ml)
- M = weight of catalyst loaded for measurement (g)
- F = flow NH_3 through reactor (mL STP/min)
- m = molar mass of NH_3 (17.03 g/mol)

4.3.5 Pyridine-IR

On a PerkinElmer 2000 apparatus, pyridine desorption from Pt/Al_2O_3 has been examined. 15 mg undilluted sample was pressed to a tablet at 3 tons. Prior to analysis, the sample is dried in vacuum at 550 °C for 1 hour. Next, pyridine is introduced in a single pulse and the system is equilibrated for 30 minutes. Physisorbed pyridine is removed via high vacuum. During a heating procedure up to 550 °C (8 °C/min), an IR spectrum between (1400-1700 cm^{-1}) of the desorption is taken every 25 °C. Obtained spectra are then normalized for pellet weight.

4.3.6 Catalytic tests

In an Avantium Flowrence 16-parallel fixed bed reactor system, the catalytic performance of the samples was examined. In these tests, 100 mg reference sample, and 50 mg of the bifunctional catalysts is loaded per fixed bed stainless steel reactor (undiluted). Prior to measurement, the catalysts are dried at 150 °C for 2 hours (He) and reduced at 300 °C for 1 hour (25% H_2/He). n-Heptane conversion is measured at 10 bar, H_2/n-C_7 = 10 and WHSV $\approx$ 0.6-1.3 h^{-1}.

The product distributions of the series of measured references and catalysts have been calculated by summing yields of certain products, according to the following formulas. Metal cracking and Secondary cracking (formula 4.4) are calculated from the same product yields. The amount of primary cracking, type B β-scission (formula 4.3), can be traced with the amount of i-C4 formed. Although propane also forms as a result of primary cracking, it does not solely originate from β-scission and can also be formed by metal cracking, overcracking or type C β-scission. Since type B β-scission is more favorable than type C β-scission, it can further be assumed that if no i-C4 product is measured, type C β-scission did not occur either. For isomerization activity, which can be ascribed to metallic platinum, the i-C7 yield is traced (formula 4.2).

Isomerization

$$\sum(i-C7) \approx 2mC6 + 3mC6 + 2,2dmC5 + 3,3dmC5 \tag{4.2}$$

Primary Cracking

$$\frac{7}{4}(i-C4) \tag{4.3}$$

Metal Cracking/Secondary cracking

$$C1 + C2 + \frac{7}{4}(nC4) + 2mC4 + n-C5 + 2mC5 + 3mC5 + nC6 \tag{4.4}$$

Chapter 5

Results and Discussion

5.1 References: Pt/Al_2O_3 and Pt/SiO_2

Results obtained related to part I of this study will be summarized. Preparation of the reference catalysts, the analysis of surface acidity and their catalytic performance is described.

5.1.1 Preparation

Preparation of Pt/Al_2O_3

In order to obtain reference samples with equal platinum particle size and weight loading, both SEA and IWI have been applied to determine the preferred synthesis method. SEA was found to be unfavorable in terms of obtaining equal weight loading and hence is not discussed in detail. However, the interested reader is referred to Appendix 9.2 for results related to this procedure.

Pt/Al_2O_3 samples with both PTA and CPA precursor have been prepared by IWI. Samples obtained showed a comparable weight loading and platinum particle size distribution: $Pt/Al_2O_3{}^{pta}$, named after the applied precursor, contained 1.3 wt.% Pt and an average platinum nanoparticle size of 1.4 nm. $Pt/Al_2O_3{}^{cpa}$ contained 1.4 wt.% Pt, with an average platinum nanoparticle size of 1.3 nm. Because in this study the catalytic performance of several samples will be compared, it is preferential to keep other parameters like synthesis procedure the same as much as possible. This will decrease factors that could influence catalytic performance like sample impurities. Since chlorine introduction was already decided to take place via IWI and IWI was successful in obtaining Pt/Al_2O_3 with both precursors, it was decided that all samples would be prepared via this route when viable. ICP-OES results, HAADF-STEM images and platinum particle size histograms are shown in Figure 5.1 for Pt/Al_2O_3 catalysts prepared both with SEA(a,b) and IWI(c,d). The catalysts prepared with IWI, Figure 5.1 c(PTA) and d(CPA), showed a narrower size distribution, higher Pt weight loading and smaller average Pt particle size compared to the SEA procedure.

The grown Pt/Al_2O_3 samples named $Pt/Al_2O_3{}^{pta}$-g (1.3 wt.% Pt) and $Pt/Al_2O_3{}^{cpa}$-g (1.4 wt.% Pt), yielded an average platinum particle size of 2.7 and 3.2 nm respectively, although $Pt/Al_2O_3{}^{pta}$-g contained a much broader size distribution than $Pt/Al_2O_3{}^{cpa}$-g. HAADF-STEM images of both grown samples and corresponding size distributions can be found in Appendix 9.3.

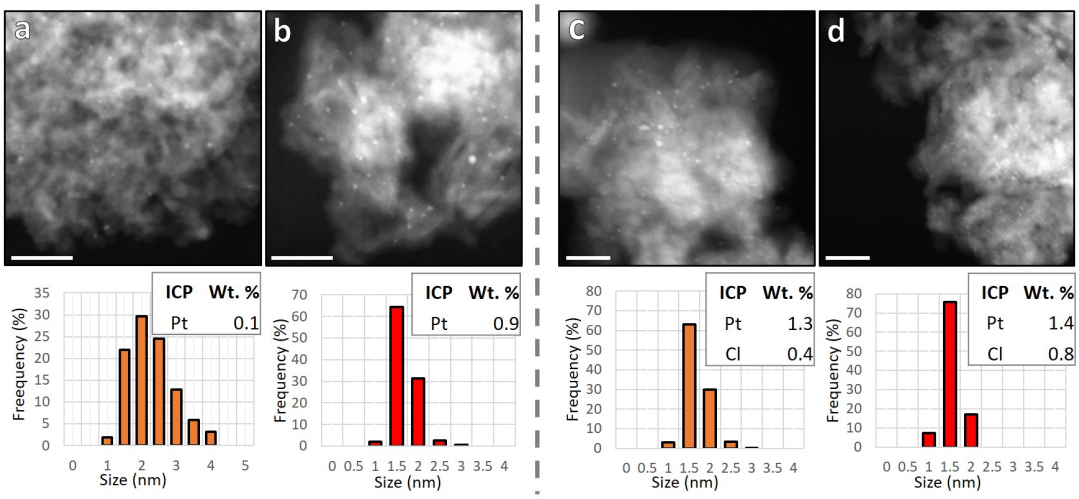

FIGURE 5.1: *Left: samples prepared via SEA, Right: samples prepared via IWI. a,c) $Pt/Al_2O_3{}^{pta}$ (orange bars). b,d) $Pt/Al_2O_3{}^{cpa}$ (red bars). Corresponding ICP-OES results and particle size histograms are summarized below the HAADF-STEM images. Scale bars are 20 nm.*

Cl impregnated Pt/Al_2O_3

The as prepared $Pt/Al_2O_3{}^{cpa}$ was additionally treated with NH_4Cl solutions to raise the chlorine content. Since ICP results of $Pt/Al_2O_3{}^{cpa}$ already indicated the presence of chlorine content before the treatments, a non treated $Pt/Al_2O_3{}^{pta}$ and $Pt/Al_2O_3{}^{cpa}$ were kept as a baseline, since chlorine content is challenging to completely remove.[48] In total, $Pt/Al_2O_3{}^{cpa}$ impregnated with 1, 3, 6, 9, 12 and 15 wt.% Cl have been prepared. Determined Pt and Cl weight loadings and average platinum particle sizes are summarized in Table 5.1. Figure 5.2 highlights HAADF-STEM results and corresponding particle size distributions obtained on some chlorine impregnated $Pt/Al_2O_3{}^{cpa}$ samples.

Samples with 1, 3 an 6 wt.% Cl (single impregnated) and samples with 9, 12 and 15 wt.% Cl (double impregnated) were prepared from the same batch of $Pt/Al_2O_3{}^{cpa}$ respectively, and hence should contain a comparable Pt weight loading. Surprisingly, the ICP-OES data show a considerable fluctuation in the measured Pt content, and also seems to increase as function of increasing amount of Cl added. In

Name	Cl wt.% (Added)	Cl wt.% (Obtained)	Pt wt.% (Obtained)	Pt np size (nm)
$Pt/Al_2O_3{}^{cpa}$	0	0.8	1.4	1.3
$Pt/Al_2O_3{}^{cpa}$(Cl-1)	1	1.0	0.7	2.5
$Pt/Al_2O_3{}^{cpa}$(Cl-3)	3	1.0	1.2	2.1
$Pt/Al_2O_3{}^{cpa}$(Cl-6)	6	1.1	1.4	2.4
$Pt/Al_2O_3{}^{cpa}$(Cl-9)	9	0.8	2.8	2.7
$Pt/Al_2O_3{}^{cpa}$(Cl-12)	12	0.9	1.5	-
$Pt/Al_2O_3{}^{cpa}$(Cl-15)	15	0.7	1.4	3.7

TABLE 5.1: *Prepared chlorine impregnated $Pt/Al_2O_3{}^{cpa}$ samples and their corresponding amount of Cl added during synthesis, obtained Cl and Pt weight loading (ICP-OES) and Pt particles size (HAADF-STEM).*

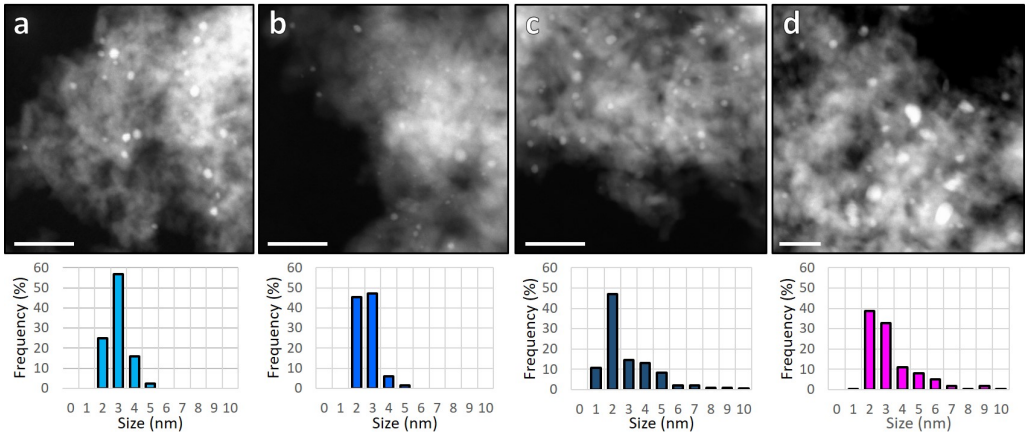

FIGURE 5.2: *HAADF-STEM images and corresponding Pt particle size distributions of a) $Pt/Al_2O_3^{cpa}$(Cl-1) (light blue), b) $Pt/Al_2O_3^{cpa}$(Cl-3) (mid blue), c) $Pt/Al_2O_3^{cpa}$(Cl-6) (dark blue) and d) $Pt/Al_2O_3^{cpa}$(Cl-9) (pink). Scale bars are 20 nm.*

the double impregnated samples, the Pt content shows an even larger fluctuation. Since a measured Pt weight content of 2.8% weight is quite extreme, considering that $Pt/Al_2O_3^{cpa}$(Cl-9) to (Cl-15 should have the same Pt weight loading, this particular measurement is assumed to be a miscalculation. When this value is excluded, the average Pt content for the double impregnated catalysts is 1.5 wt.%. For the single impregnated catalysts, although the obtained platinum weight content is in the anticipated range, metallic platinum is not expected to desorb from the surface, explaining the loss of platinum in the single impregnated samples. For this reason, also the Pt content of the single impregnated references is calculated as the average of the three measured values: 1.1 wt.% Pt.

The amount of obtained Cl increases slightly in the single impregnated samples from 1.0 to 1.1 wt.% as function of added Cl during the impregnation. The double impregnated samples show no clear trend in Cl content. The high temperature aftertreatment of the chlorinated samples is expected to remove most of the introduced chlorine, in accordance with a comparable study.[47] The ICP-OES values obtained on Cl content are therefore in expected range, but the variations indicate that this technique alone might not be appropriate for precise quantification of especially Cl in the prepared samples.

In Figure 5.2 it is observed that Pt particle size distribution broadens as function of added Cl content. Especially in the single impregnated samples, it is observed that also a small fraction of smaller Pt nanoparticles form, which could indicate that the particle growth is caused by Ostwald Ripening. In a recent study by Liu *et al.*, on the effect of NaCl present during the synthesis of Pt/Al_2O_3 catalysts, it was observed that a higher amount of chlorine resulted in larger Pt nanoparticles on a variety of supports. In the paper it was demonstrated that the addition of Cl^- or NO_3^- could be used as a method to enhance the Pt particle growth.[61] Other research has attributed this growth to the formation and agglomeration of $H_xPt_yCl_z$ cluster intermediates.[54] In this study, the chlorine is introduced in a separate step, after the synthesis of $Pt/Al_2O_3^{cpa}$. The Pt nanoparticles should therefore be anchored to the support in a metallic state during the addition of NH_4Cl. However, the observed particle growth indicates that the chlorine induces the Pt nanoparticles to become mobile to a certain degree.

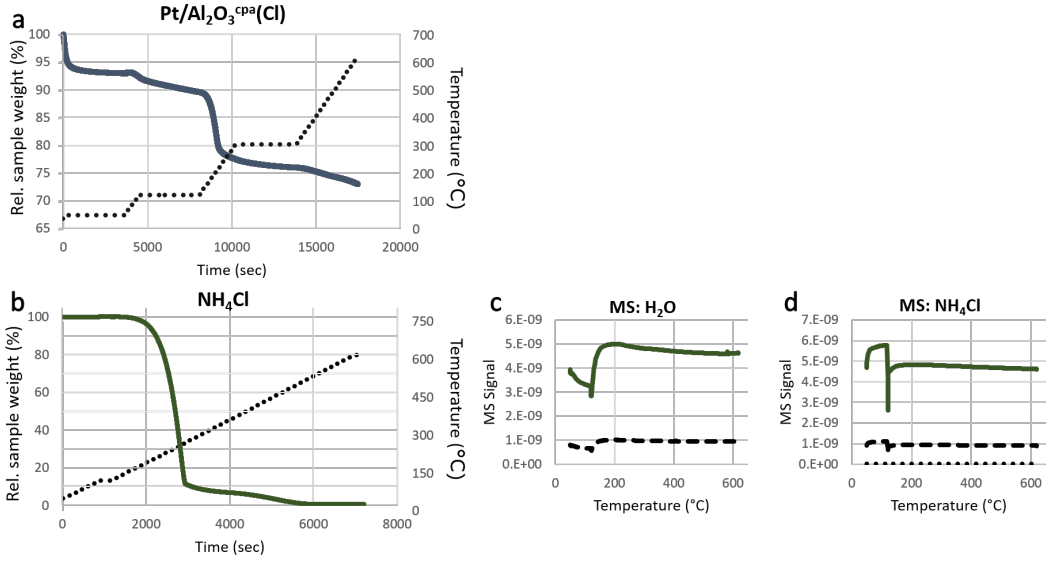

FIGURE 5.3: *Relative sample weight and reactor temperature (black dotted) as function of time for a) $Pt/Al_2O_3^{cpa}(Cl)$ (blue) and b) NH_4Cl (green). MS data of the NH_4Cl sample for c) H_2O: 18 m/z (solid) and 17 m/z (dashed) and d) NH_4Cl: 36 m/z (solid), 38 m/z (dashed) and 35 m/z (dotted).*

In order to examine at which temperature chlorine is desorbing from the impregnated samples during the heat treatment, a non aftertreated, $Pt/Al_2O_3^{cpa}$ sample impregnated with a saturated NH_4Cl solution, named $Pt/Al_2O_3^{cpa}(Cl)$, was studied with TGA-MS. M/z ratios corresponding to H_2O: 18 (100%), 17 (20%) m/z, NH_3: 16 (80%) m/z, HCl: 36 (100%), 38 (30%) m/z and Cl_2: 70 (100%) m/z were analyzed during a temperature ramp up to 600 °C. It was observed that the sample decreases more than 10% in weight around 200 °C, which is shown in Figure 5.3a. At increasing temperature the mass of the sample keeps decreasing, although after 250 °C this loss is more gradual. Combined with the obtained MS data this drop could not be related to the loss of any of the measured compounds. Possibly the MS was not sensitive enough for this detection. The MS data did indicate that NH_3 and H_2O were desorbing from the sample, but this signal did not correspond to the weight drop. An overview of the MS plots of this sample is included in Appendix 9.4.

Also, a pure NH_4Cl sample has been studied with TGA-MS to measure the sublimation point, which was determined to be 200-220 °C, as shown in Figure 5.3b. The obtained MS signals on H_2O, and NH_4Cl from this measurement, as shown in Figure 5.3c and d further indicated that the applied NH_4Cl contained significant water content. The measured weight drop of $Pt/Al_2O_3^{cpa}(Cl)$, which occurred at comparable temperature as the sublimation, could have been caused by the sublimation of NH_4Cl.

Preparation of Pt/SiO_2

As an extra reference catalysts, Pt/SiO_2^{pta} was prepared. The sample had lower Pt loading, contained 1.1 wt.% Pt and 0.6 wt.% Cl. The average Pt particle size was 1.4 nm. Silica has much lower affinity to chlorine,[53] but ICP-OES did not show this feature. However, results obtained on a previously analyzed Pt/SiO_2, which was prepared via the same described method, contained 0.7 wt.% Pt and 0.1 wt.% Cl. This would agree with reported Cl affinity of silica, when $Pt/Al_2O_3^{pta}$ (Figure 5.1c)

and Pt/SiO_2^{pta} are compared since they both should, in theory, be chlorine free. Particle size distribution and TEM/HAADF-STEM results are depicted in Appendix 9.3.

5.1.2 Support Acidity Analysis

In order to elucidate the contribution of chlorine to the support acidity, a wide variety of samples has been analyzed with NH_3-TPD or pyridine-IR. Results are presented per technique.

NH_3-TPD

In NH_3-TPD measurements the surface acidity the reference materials was examined. In Figure 5.4a, the TCD signal of Pt/SiO_2^{pta} (brown), $Pt/Al_2O_3^{pta}$ (orange) and $Pt/Al_2O_3^{cpa}$ (red) is plotted against the temperature, with an extra pure γ-alumina sample (gray) and Zeolite Y CBV760 sample (black/dotted) as a control. Both Pt/Al_2O_3 catalysts have a lower TCD signal than the γ-alumina reference up to 340 °C, indicating that both catalysts have a lower amount of weak acidic sites compared to the pure support. Most likely some of the acidity is lost due to small Pt nanoparticles covering the surface. Another factor is the slight basic properties that Pt particles smaller than 1.5 nm exhibit as a result of unfilled metallic bands. The nanoparticles are then more prone to donate electrons and with that the acidic properties of alumina are moderately compensated.[54] At elevated temperatures, both catalysts show a higher TCD signal, indicating a larger amount of strong acidic surface sites. When the profile of $Pt/Al_2O_3^{pta}$ is compared to $Pt/Al_2O_3^{cpa}$ it is observed that $Pt/Al_2O_3^{cpa}$ has a slightly higher TCD signal in the weak acidic site region. This can be the consequence of the residual chlorine atoms in this sample due to the precursor, but overall the plots of $Pt/Al_2O_3^{pta}$ and $Pt/Al_2O_3^{cpa}$ are certainly comparable. $Pt\text{-}SiO_2^{pta}$ displayed a low desorption signal, which is coherent with the non acidic properties of silica. The Zeolite Y reference shows well distinguishable signals in the weak and strong acid site region compared to the alumina samples. However, the overall intensity is rather low compared to the Pt/Al_2O_3 samples, even though zeolite is known to be much more acidic than alumina.

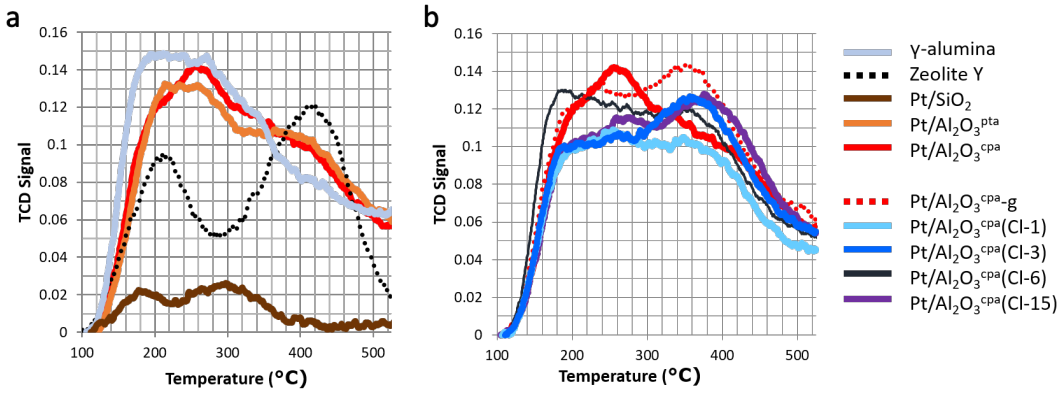

FIGURE 5.4: *a) NH_3-TPD profiles of $Pt/Al_2O_3^{pta}$ (orange), $Pt/Al_2O_3^{cpa}$ (red) and $Pt\text{-}SiO_2^{pta}$ (brown) compared to a γ-alumina reference (gray) and CBV760 sample (black/dotted). b) NH_3-TPD profiles of $Pt/Al_2O_3^{cpa}$ (red), $Pt/Al_2O_3^{cpa}$-g (red/dotted) and the chlorine impregnated samples $Pt/Al_2O_3^{cpa}$(Cl-1) (light blue), $Pt/Al_2O_3^{cpa}$(Cl-3) (mid blue), $Pt/Al_2O_3^{cpa}$(Cl-6) (dark blue) and $Pt/Al_2O_3^{cpa}$(Cl-15) (purple).*

Name	total NH_3 des ml/g cat (abs)	SAS NH_3 des ml/g cat (abs)	ml/g cat (rel)	mmol/g cat (rel)
Pt/SiO_2^{pta}	2.4	1.5		
Zeolite Y (CBV760)	16.3	10.1		
γ-alumina (pure)	18.6	7.5		
$Pt/Al_2O_3^{pta}$	22.2	11.5	4.0	0.18
$Pt/Al_2O_3^{cpa}$	22.7	11.9	4.3	0.20
$Pt/Al_2O_3^{cpa}$-g	19.1	13.4	5.9	0.27
$Pt/Al_2O_3^{cpa}$(Cl-1)	16.3	12.8	5.3	0.24
$Pt/Al_2O_3^{cpa}$(Cl-3)	18.1	15.7	8.2	0.37
$Pt/Al_2O_3^{cpa}$(Cl-6)	17.7	13.9	6.4	0.29
$Pt/Al_2O_3^{cpa}$(Cl-9)	19.0	15.1	7.6	0.34
$Pt/Al_2O_3^{cpa}$(Cl-12)	18.5	14.2	6.7	0.30
$Pt/Al_2O_3^{cpa}$(Cl-15)	18.6	14.9	7.3	0.33

TABLE 5.2: *Amount of total NH_3-desorption in ml/g catalyst, amount of NH_3 desorption from strong acid sites SAS in ml/g catalysts and mmol/g catalyst. Values are also given relative (rel) to the γ-alumina data.*

The chlorine impregnated $Pt/Al_2O_3^{cpa}$ samples were also analyzed with NH_3-TPD, including $Pt/Al_2O_3^{cpa}$-g as an extra control to study the effect of particle size on surface acidity. A highlight of this is given in Figure 5.4b. When the $Pt/Al_2O_3^{cpa}$ (red) catalyst is impregnated with 1 wt.% (light blue) or 3 wt.% (mid blue) Cl, the high temperature desorption peak increases, indicating a larger amount of strong acid sites. The $Pt/Al_2O_3^{cpa}$(Cl-6) (dark blue) shows an enhanced amount of strong acid sites compared to the non impregnated catalyst, but also has increased TCD signal at the weak acid site region. Furthermore it was observed that the double NH_4Cl impregnated catalyst, did not show a further increase in strong acid site signal and the plots of $Pt/Al_2O_3^{cpa}$(Cl-9), $Pt/Al_2O_3^{cpa}$(Cl-12) and $Pt/Al_2O_3^{cpa}$(Cl-15) were very comparable. For this reason, only the $Pt/Al_2O_3^{cpa}$(Cl-15) is presented out of those, but all double impregnated samples are presented in Appendix 9.5. It could indicate that these samples did not contain a higher amount of chlorine, which would be in agreement with the represented ICP data. The data of the $Pt/Al_2O_3^{cpa}$-g (red/dotted) shows a remarkable TCD signal in the strong acid site region. This could indicate that the measured increase in TCD signal in the chlorine impregnated $Pt/Al_2O_3^{cpa}$ catalysts is also caused by their observed particle growth.

With the NH_3-TPD data, the NH_3 desorption from the strong acid sites was calculated. Obtained values are summarized in Table 5.2. It should be noted that all samples have a higher amount of desorption compared to literature. Zečević and coworkers reported a total NH_3 desorption of 14.7 ml/g catalyst for a $Pt/Al_2O_3/Y$ composite.[15] Such a sample, in which much more acidic sites are present due to the zeolite material, will certainly have greater acidity than a γ-alumina support. Also in comparison to other studies, in which NH_3-TPD results on Pt/Al_2O_3 related samples are presented it can be observed that the in this study reported values are elevated.[62,63] In order to verify that only ammonia was desorbing, a $Pt/Al_2O_3^{cpa}$ sample was measured twofold. The signal between these two measurements only showed marginal differences, indicating that during the measurements only ammonia was measured and no other inorganic compounds were desorbing from the surface. The elevation in measured TCD signal might then come from physisorbed

ammonia on the support. When the TCD signal of γ-alumina is compared to Zeolite Y from Figure 5.4, it is observed that only the desorption below 360 °C is increased. Although at such a temperature physisorbed ammonia should not be present, the calculated data are most unlikely. Quantification via a 3 peak deconvolution might not be the most viable method for alumina supported samples.

As a reference to the TPD data, a pure γ-alumina sample was analyzed. The amount of NH_3-desorption is also depicted relative to this value in the (rel) columns. It can be seen that the introduction of Pt nanoparticles on the alumina surface results in increased NH_3-desorption, which is in accordance with literature.[63] Introduction of Cl, results in a further increase of NH_3-desorption from the strongly acidic sites, although a clear trend is not readily observed. The deconvoluted spectra applied in the quantification can be found in Appendix 9.5.

When the total amount of desorbed ammonia is compared between the samples, it is seen that although the double chlorine impregnated samples have roughly the same amount of desorption as the γ-alumina reference, the single impregnated catalyst have a decreased desorption. If indeed the single impregnated samples contain more chlorine than the double impregnated samples, which is in accordance with ICP, this could indicate that chlorine located on the surface inhibits the adsorption (physisorption) of ammonia, since there are less surface hydroxyl groups present. Furthermore, the $Pt/Al_2O_3{}^{pta}$ and $Pt/Al_2O_3{}^{cpa}$ samples have a notable enhanced total desorption of ammonia, which could contribute to the higher calculated amount of strong acid sites.

Pyridine-IR

Pyridine-IR measurements have been performed on the $Pt/Al_2O_3{}^{pta}$ and $Pt/Al_2O_3{}^{cpa}$ catalysts, in order to verify if the residual chlorine from synthesis would have a measurable effect on the support surface brønsted and lewis acidity. Figure 5.5 presents the obtained pyridine-IR desorption data from 50 to 550 °C for both samples. Although the differences between both samples are very subtle, and therefore not applicable for quantification, it can be observed that the CPA prepared catalyst (solid lines) has a higher intensity, which indicates a higher amount of strong acidic sites. Both intensity of brønsted acid sites (BAS) and lewis acid sites (LAS) is slightly increased, even though chlorine impregnation is considered to mainly affect the brønsted acidity of the support as a result hydroxyl group substitution. However, an increase in strong lewis acidity is in accordance with the proposed chlorine positions by Guillaume *et al*, which as described in Chapter 2.2.[50]

The most prominent difference between the two reference samples is observed in the peak shoulder at 1620 cm^{-1}, which is characteristic for brønsted acid sites. This difference however quickly fades when the desorption temperature reaches 450 °C. Furthermore, at the lower desorption temperatures, the CPA sample shows a very small signal around 1540 cm^{-1}, which is characteristic for strong brønsted acid sites. This peak has a combination band at 1643 cm^{-1}, which is also slightly visible in the presented data.[64,65] Although this signal is very weak, it is not visible in the PTA prepared sample (dotted lines) and hence shows that small distinctions can be made between both catalysts. Minor differences in acidic properties between $Pt/Al_2O_3{}^{pta}$ and $Pt/Al_2O_3{}^{cpa}$ as a result of residual chlorine can therefore be assumed.

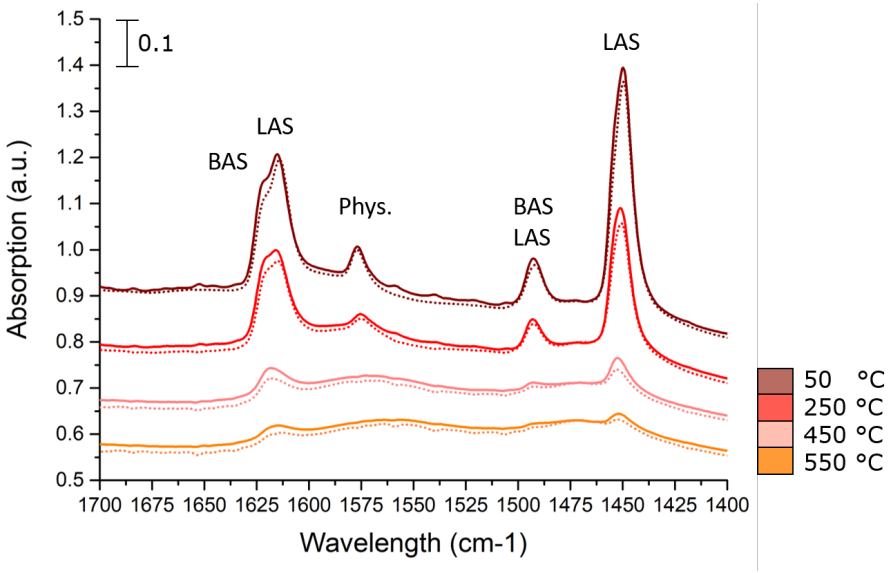

FIGURE 5.5: *Pyridine-IR desorption graphs of $Pt/Al_2O_3^{pta}$ (dotted) and $Pt/Al_2O_3^{cpa}$ (solid) at 50, 250, 450 and 550 °C, with an offset of 0.1. Baseline is set at 1475 cm-1.*

5.1.3 Catalytic Performance

The Pt/Al_2O_3 and chlorine impregnated $Pt/Al_2O_3^{cpa}$ references have been tested in terms of catalytic activity, selectivity and stability.

Catalyst Activity

Of the reference samples, the activity of Pt/SiO_2^{pta}, $Pt/Al_2O_3^{pta}$, $Pt/Al_2O_3^{cpa}$ and the samples with increased platinum particle size $Pt/Al_2O_3^{pta}$-g and $Pt/Al_2O_3^{cpa}$-g has been examined, shown in Figure 5.6a. It can be seen that the non grown reference samples have comparable activity, and that $Pt/Al_2O_3^{pta}$ has a lower activity compared to $Pt/Al_2O_3^{cpa}$. Pt/SiO_2^{pta}, lacking strong acidic sites in general, should have no n-heptane conversion arising from a bifunctional mechanism. However, it shows a surprising activity compared to the Pt/Al_2O_3 references, although the sample did not show a smaller average platinum particle size. A plausible explanation is that Pt/SiO_2^{pta} could have significant conversion as a result of mainly metal cracking, which was described in Chapter 2. This mechanism is also assumed to contribute to the activity of the Pt/Al_2O_3 references. The grown samples, exhibiting less metallic platinum surface area, show a lower overall n-heptane conversion as function of reactor temperature.

In the chlorine impregnated $Pt/Al_2O_3^{cpa}$, which are shown in Figure 5.6b, it is observed that a higher amount of added chlorine in the impregnation step, results in a decrease of total catalytic activity in case of the single impregnated samples (blue lines). For the double impregnated catalysts, of which only the $Pt/Al_2O_3^{cpa}$(Cl-15) has been highlighted, since these samples showed the same temperature dependence, the catalytic activity did not follow a comparable trend to the single impregnated references. It should be noted that an increase in chlorine content in the treatment also resulted in larger platinum nanoparticles and that these samples are more comparable in activity to the grown Pt/Al_2O_3 references.

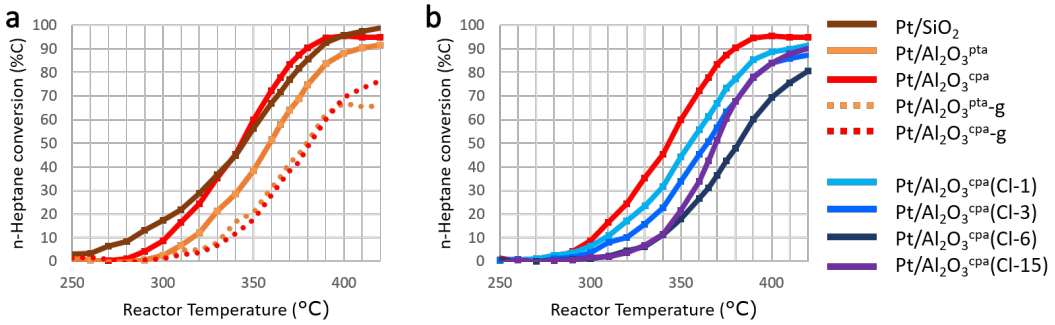

FIGURE 5.6: *n-Heptane conversion as function of reactor temperature. a) Pt/SiO_2^{pta} (brown), $Pt/Al_2O_3^{pta}$ (orange), $Pt/Al_2O_3^{cpa}$ (red), $Pt/Al_2O_3^{pta}$-g (orange/dotted) and $Pt/Al_2O_3^{cpa}$ (red/dotted). b) Chlorine impregnated samples compared to $Pt/Al_2O_3^{cpa}$ (red): $Pt/Al_2O_3^{cpa}$(Cl-1) (light blue), $Pt/Al_2O_3^{cpa}$(Cl-3) (mid blue), $Pt/Al_2O_3^{cpa}$(Cl-6) (dark blue) and $Pt/Al_2O_3^{cpa}$(Cl-15) (purple)*

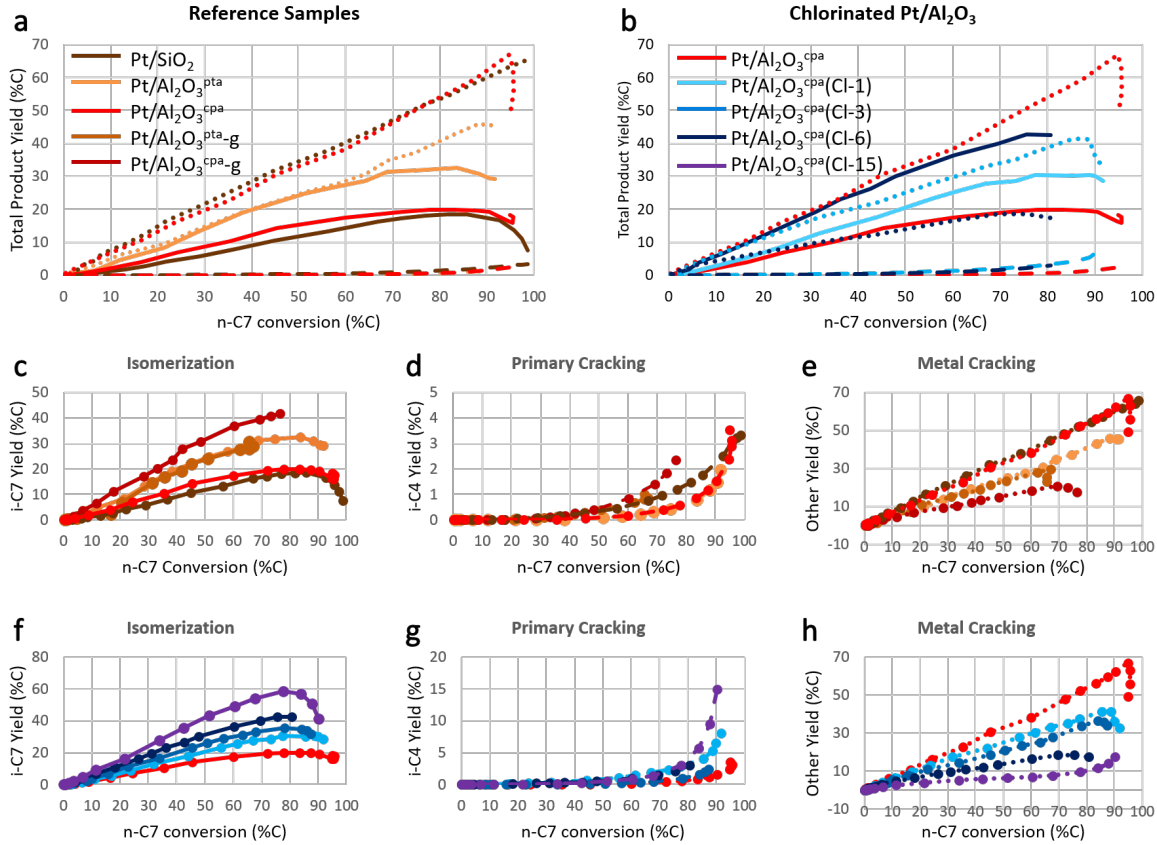

FIGURE 5.7: *Product distributions for: a) Reference samples Pt/SiO_2^{pta}(brown), $Pt/Al_2O_3^{pta}$(orange), $Pt/Al_2O_3^{cpa}$(red). b) Chlorine containing samples $Pt/Al_2O_3^{cpa}$(red), $Pt/Al_2O_3^{cpa}$(Cl-1) (light blue) and $Pt/Al_2O_3^{cpa}$(Cl-6) (dark blue). 5.7c,d,e) Detailed yields of the reference samples for Isomerization (solid), Primary cracking (dashed) and Metal cracking (dotted). Reference samples $Pt/Al_2O_3^{pta}$-g (ocher) and $Pt/Al_2O_3^{cpa}$-g(dark red) are also included. 5.7f,g,h) Detailed yields of the chlorine containing samples, in which also $Pt/Al_2O_3^{cpa}$(Cl-3) (mid blue) and $Pt/Al_2O_3^{cpa}$(Cl-15) (purple) are included.*

Catalyst Selectivity

In Figure 5.7, the selectivities of the prepared reference catalysts for isomerization, primary cracking and metal cracking are presented. A highlight of this is shown in Figure 5.7a and 5.7b. As can be seen in figure 5.7a, in which the total product yields of Pt/SiO_2^{pta}, $Pt/Al_2O_3^{pta}$ and $Pt/Al_2O_3^{cpa}$ are depicted, the samples have only very limited bifunctional activity (dashed lines), considering the low primary cracking yield. Pt/SiO_2^{pta} and $Pt/Al_2O_3^{cpa}$ are highly comparable in both isomerization (solid lines) and metal cracking (dotted lines). However, in $Pt/Al_2O_3^{pta}$, a significantly higher amount of isomerization is observed at the cost of metal cracking yield. The ICP results showed that $Pt/Al_2O_3^{pta}$ had a slightly lower weight loading compared to $Pt/Al_2O_3^{cpa}$ (1.3 wt.% and 1.4 wt.% Pt respectively), which could have influenced the amount of metal cracking occurring between these samples, since metal cracking is considered to only be catalyzed by the platinum metallic function. The product distribution of Pt/SiO_2^{pta}, which measured a platinum loading of 1.1 wt.%, cannot be described with the same reasoning. However, since silica and alumina supports have chemically very different properties, such a comparison might also not be justifiable and other effects, not examined in this study, might play a more determining role.

Figure 5.7b illustrates the product distribution of $Pt/Al_2O_3^{cpa}$ impregnated with 1 wt.% Cl and 6 wt.% Cl, compared to the non chlorinated catalyst. An increase in introduced chlorine content results in more isomerization at the cost of metal cracking. In sub-figures 5.7f, g and h, in which also 3 wt.% Cl and 15 wt.% Cl samples are included, this trend is continued. Furthermore, the Cl-15 sample shows that a higher introduced chlorine content results in more bifunctional activity compared to the non chlorinated $Pt/Al_2O_3^{cpa}$ sample. Previously reported ammonia-TPD and ICP data on these chlorinated samples indicated that a higher degree of impregnation with chlorine did not necessarily result in stronger surface acidity or higher chlorine content. The observed differences can therefore be caused by the fact that chlorine impregnated samples include a bigger platinum particle size. For this reason, the grown reference samples are included in sub-figures 5.7c,d and e. Indeed it is observed that the larger average particle size of $Pt/Al_2O_3^{cpa}$-g results in more isomerization at the cost of metal cracking, comparable to the chlorine impregnated samples.

In order to examine the particle size effects in more detail, the metal cracking turn over frequency (TOF) has been calculated, normalized for the amount of surface platinum (mol). The samples showed comparable results below 350 °C, except for Pt/SiO_2^{pta}. The calculation procedure and obtained metal cracking TOF results can be found in Appendix 9.6.

Catalyst Stability

As an extra measurement the samples were tested at 325 °C after the high temperature measurements, in order to examine the amount of deactivation.

First of all, the reference samples were deactivating considerably and the chlorine impregnation step seemed to influence the total amount of deactivation, although a clear trend was not observed. The single chlorine impregnated samples roughly indicate that higher concentrations result in more deactivation, while the double chlorine impregnated samples did not follow such a trend and even more activity was measured (not shown). Surprisingly, there was significant difference in deactivation

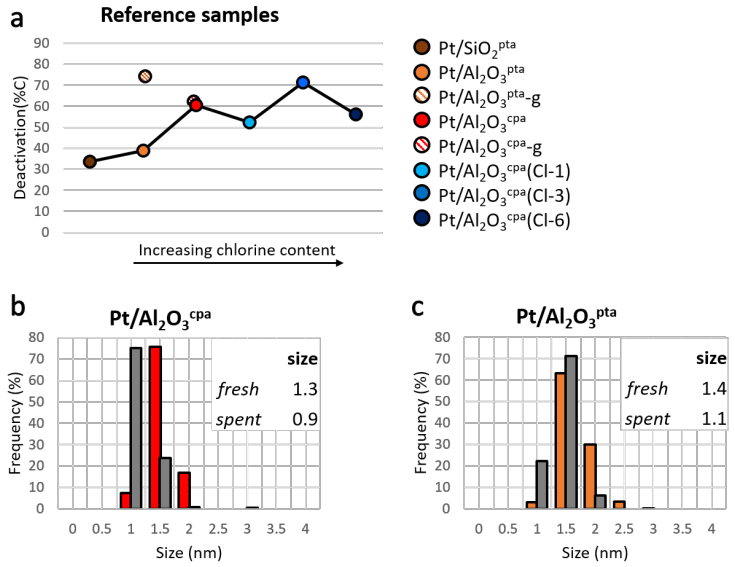

FIGURE 5.8: *a) Deactivation of reference samples, measured at 325 °C, compared to initial conversion. b) Average platinum particle size (nm) and distribution for fresh (red) and spent (gray) $Pt/Al_2O_3^{cpa}$. c) average platinum particle size (nm) and distribution for fresh (orange) and spent (gray) $Pt/Al_2O_3^{pta}$.*

between the grown references Pt/ $Al_2O_3^{pta}$-g and $Pt/Al_2O_3^{cpa}$-g. As function of increasing platinum particle size, $Pt/Al_2O_3^{pta}$-g seems to a higher extend compared to $Pt/Al_2O_3^{cpa}$-g. The deactivation of the reference samples is shown in Figure 5.8a, up to the single impregnated catalysts.

In order to examine the cause of the observed deactivation, the average platinum particle size has been determined of spent catalysts $Pt/Al_2O_3^{pta}$ and $Pt/Al_2O_3^{cpa}$. The average platinum particle size of these samples was lower than the freshly prepared ones, as shown in Figure 5.8b and c. A decreasing particle size could be a sign of Ostwald Ripening, but the obtained size distribution from the spent catalyst was not broader than fresh catalysts and hence Ostwald Ripening cannot explain this finding. Nanoparticles with a diameter below ∼1.5 nm are challenging to visualize with TEM analysis. It might have been that the fresh catalysts were also including such small particles, but that in this measurement they were not visible.

To verify if coke formation was the cause of deactivation, the spent reference catalysts were visually compared to fresh references. The spent Pt/Al_2O_3 samples were all slightly darker, which is indicative for coking by a non ideal process. This is shown in Figure 5.9.

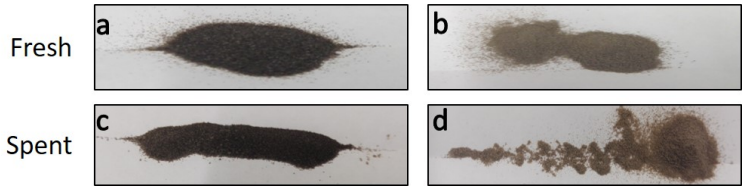

FIGURE 5.9: *Images of the fresh and spent catalysts a) fresh $PtAl_2O_3^{cpa}$, b) fresh $PtAl_2O_3^{cpa}$(Cl-15), c) spent $PtAl_2O_3^{cpa}$ and d) spent $PtAl_2O_3^{cpa}$(Cl-6). It is noted that b and d are not images from the same sample. However, fresh chlorine impregnated reference samples were all very comparable in color.*

5.2 Bifunctional Catalysts: Pt/Al_2O_3/Zeolite Y

5.2.1 Preparation

The millimeter scale and microscale bifunctional catalysts, named $Pt/Al_2O_3{}^{cpa}$/Y-pm and $Pt/Al_2O_3{}^{cpa}$/Y-ipm respectively, have been prepared out of the Pt/Al_2O_3 reference samples and are therefore not additionally measured with TEM/HAADF-STEM or ICP. For this reason, only results related to the preparation of nanoscale intimate samples are presented.

Preparation of Pt/Al_2O_3/Y-comp

The nanoscale bifunctional catalysts, $Pt/Al_2O_3{}^{cpa}$/Y-comp, are prepared in a separate SEA procedure, and have been impregnated with NH_4Cl solutions corresponding to 1 wt.% Cl and 6 wt.% Cl, in a single impregnation from the same batch, yielding $Pt/Al_2O_3{}^{cpa}$/Y(Cl-1)-comp and $Pt/Al_2O_3{}^{cpa}$/Y(Cl-6)-comp respectively. ICP-OES measurements on $Pt/Al_2O_3{}^{cpa}$/Y-comp indicated 0.7 wt.% Pt and 0.8 wt.% Cl. Due to the fluctuations in obtained ICP data on the references, $Pt/Al_2O_3{}^{cpa}$/Y(Cl-1)-comp and $Pt/Al_2O_3{}^{cpa}$/Y(Cl-6)-comp were not additionally measured on Cl content, but it was assumed to be higher than in $Pt/Al_2O_3{}^{cpa}$/Y-comp.

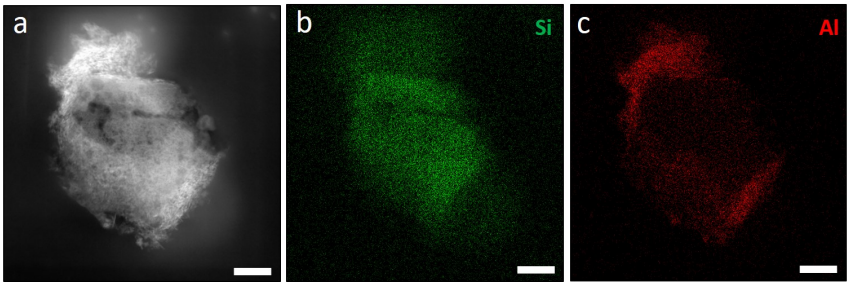

FIGURE 5.10: *Overview of distribution of Zeolite and Alumina phase in the prepared composite. a) HAADF-STEM image of the composite, b) EDX map of same region for Si (green), c) EDX map of same region for Al (red). Scale bars are 100 nm.*

The prepared composite contained regions of zeolite and alumina phase, in close proximity. This is shown in the EDX maps in Figure 5.10, in which silicon is indicative for zeolite, while aluminum is indicative for pure γ-alumina phase. The non chlorine impregnated sample, $Pt/Al_2O_3{}^{cpa}$/Y-comp, contained platinum selectively deposited on the alumina phase with a small size distribution. The average platinum particle size was 1.3 nm. However, impregnation with chlorine in these materials resulted in platinum growth and platinum relocation: both the zeolite phase and alumina phase included platinum nanoparticles and the average platinum particle size was 1.9 nm. Figure 5.11 highlights HAADF-STEM results and corresponding nanoparticle size distributions of $Pt/Al_2O_3{}^{cpa}$/Y-comp and $Pt/Al_2O_3{}^{cpa}$(Cl-1)/Y-comp.

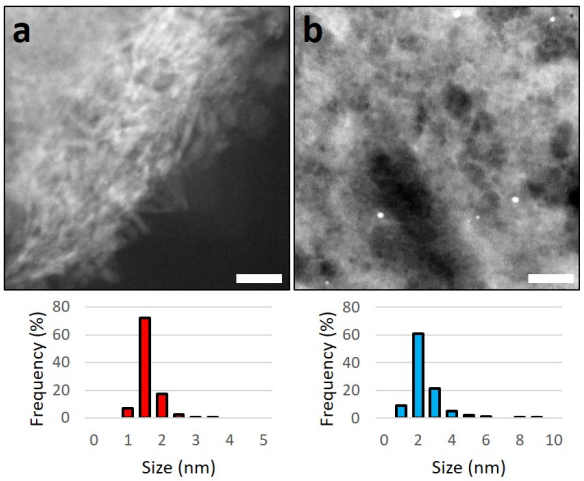

FIGURE 5.11: *Highlight of HAADF-STEM results and corresponding platinum particle size analysis for a) $Pt/Al_2O_3^{cpa}$/Y-comp (red) and b) $Pt/Al_2O_3^{cpa}$(Cl-1)/Y-comp (light blue). Scale bars are 20 nm.*

5.2.2 Catalytic Performance

The catalytic performance of the various bifunctional catalysts with ranging intimacies has been studied and results related to the activity, selectivity and stability are summarized.

Catalyst Activity

The activity of the samples is depicted in Figure 5.12. It is observed that a higher degree of intimacy also results in a higher catalytic activity at lower reactor temperatures. Furthermore, introduction of chlorine (dotted lines) to these zeolite containing samples does not significantly change the catalytic activity in case of millimeter scale (black) and microscale (mid gray) intimate samples. In these two intimacies, chlorine is added to the Pt/Al_2O_3 component, prior to mixing with the zeolite Y. In the nanoscale intimate sample (light gray), it is observed that the addition of chlorine content decreases the catalytic activity. Chlorine was added non specifically in these samples so a cause of this decrease might be that chlorine poisons the zeolite Y component. Furthermore, the HAADF-STEM results indicated Pt nanoparticle relocation and growth, which could also influence catalytic activity.

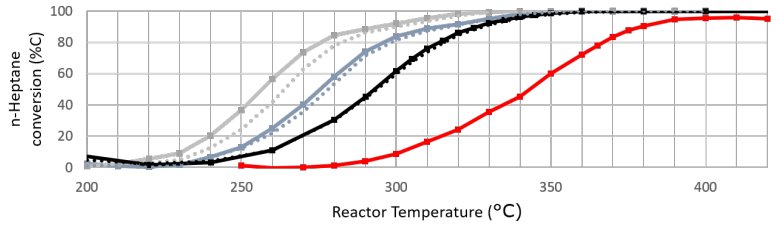

FIGURE 5.12: *n-Heptane conversion as function of reactor temperature for bifunctional catalysts with different intimacies: red= $Pt/Al_2O_3^{cpa}$ reference, black = millimeter scale intimacy: solid = $Pt/Al_2O_3^{cpa}$/Y-pm, dotted = $Pt/Al_2O_3^{cpa}$(Cl-9)/Y-pm, gray = microscale intimacy: solid= $Pt/Al_2O_3^{cpa}$/Y-ipm, $Pt/Al_2O_3^{cpa}$(Cl-6)/Y-ipm, light gray = nanoscale intimacy: solid = $Pt/Al_2O_3^{cpa}$/Y-comp, dotted = $Pt/Al_2O_3^{cpa}$(Cl-6)/Y-comp.*

Catalyst Selectivity

The zeolite based bifunctional catalysts showed less influence of chlorine content on the isomerization and metal cracking product yields. Furthermore, this influence decreased when the intimacy was increased from millimeter scale in the physical mixtures, to a nanoscale in the composites.

Millimeter scale: Pt/Al_2O_3/Y-pm

The product distribution of the physical mixtures is depicted in Figure 5.13. It is observed that a lower i-C7 yield (solid lines/outlined squares) is obtained as a result of an increased introduced chlorine content from $Pt/Al_2O_3{}^{pta}$/Y-pm (orange) and $Pt/Al_2O_3{}^{cpa}$/Y-pm (red) to the chlorine impregnated samples $Pt/Al_2O_3{}^{cpa}$(Cl-9)/Y-pm (pink) and $Pt/Al_2O_3{}^{cpa}$(Cl-15)/Y-pm (purple). In the primary cracking (dashed lines/filled squares), this increase results in a slightly higher yield, although the samples are quite comparable. The secondary cracking product formation (dotted lines/open squares) does not significantly alter.

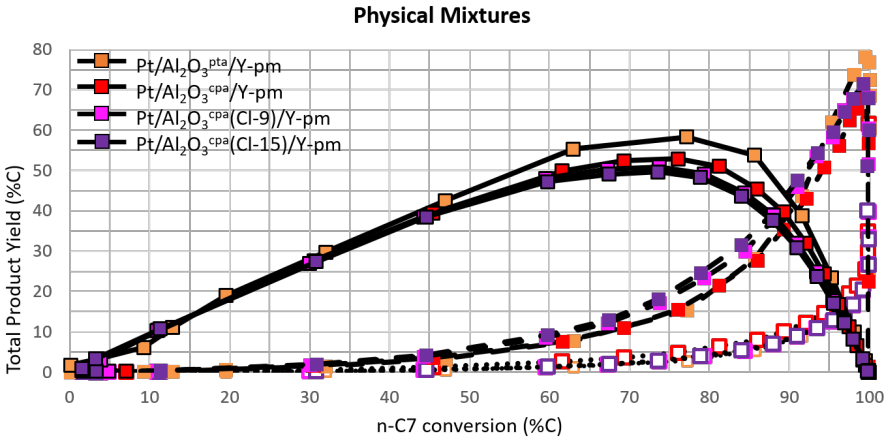

FIGURE 5.13: *Obtained product distribution in terms of isomerization (solid lines, filled/outlined symbols), primary cracking (dashed lines, filled symbols) and secondary cracking (dotted lines, open symbols) for Physical mixtures: $Pt/Al_2O_3{}^{pta}$/Y-pm (orange), $Pt/Al_2O_3{}^{cpa}$/Y-pm (red), $Pt/Al_2O_3{}^{cpa}$(Cl-9)/Y-pm (pink) and $Pt/Al_2O_3{}^{cpa}$(Cl-15)/Y-pm (purple)*

Microscale: Pt/Al_2O_3/Y-ipm

The intimate physical mixtures, depicted in 5.14, show very limited chlorine influence compared to the millimeter scale intimacy samples: non impregnated samples $Pt/Al_2O_3{}^{pta}$/Y-ipm (orange) and $Pt/Al_2O_3{}^{cpa}$/Y-ipm (red) show the same product distributions as chlorine containing samples $Pt/Al_2O_3{}^{cpa}$(Cl-1)/Y-ipm (light blue) and $Pt/Al_2O_3{}^{cpa}$(Cl-6)/Y-ipm (dark blue). When the primary cracking selectivities are compared, it is observed that the chlorine impregnated samples have a slightly higher primary cracking at lower C7 conversion. However, these values only vary roughly 1% in total yield compared to the non impregnated samples, hence are not of significant value. Compared to the physical mixtures, the intimate physical mixtures show an increased selectivity towards isomerization.

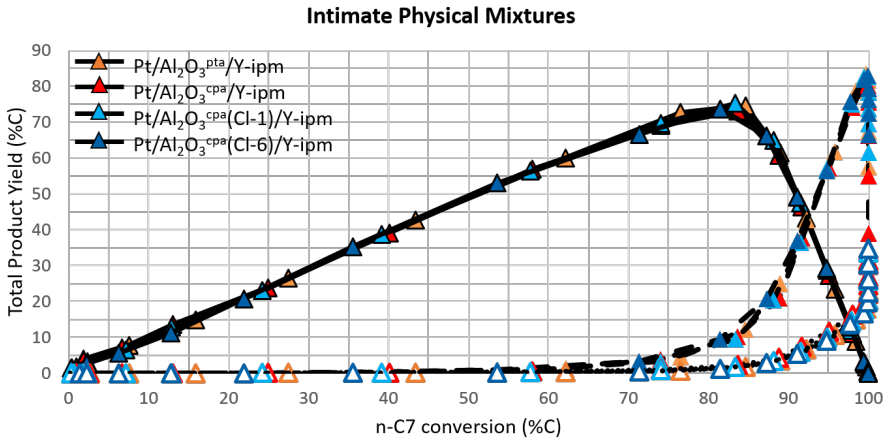

FIGURE 5.14: *Obtained product distribution in terms of isomerization (solid lines, filled/outlined symbols), primary cracking (dashed lines, filled symbols) and secondary cracking (dotted lines, open symbols) for Intimate physical mixtures: $Pt/Al_2O_3^{pta}$/Y-ipm (orange), $Pt/Al_2O_3^{cpa}$/Y-ipm (red), $Pt/Al_2O_3^{cpa}$(Cl-1)/Y-ipm (light blue) and $Pt/Al_2O_3^{cpa}$(Cl-6)/Y-ipm (dark blue).*

Nanoscale: Pt/Al_2O_3/Y-comp

In the composite materials, presented in 5.15, a variation in isomerization, primary cracking and secondary cracking between the samples is not observed. In here $Pt/Al_2O_3^{cpa}$/Y-comp (red), $Pt/Al_2O_3^{cpa}$(Cl-1)/Y-comp (light blue) and $Pt/Al_2O_3^{cpa}$(Cl-6)/Y-comp (dark blue) describe the same product distribution. The composite materials show the highest amount of primary cracking compared to the different intimacies. This is visualized in Figure 5.16a, in which it can be seen that an increased intimacy results in decrease of conversion temperature and increase of i-C4 cracking yield. Furthermore, the data indicate that chlorine impregnation also results in a slower decrease in i-C4 yield at higher reactor temperatures, but overall, the influence of chlorine on highly intimate samples is limited.

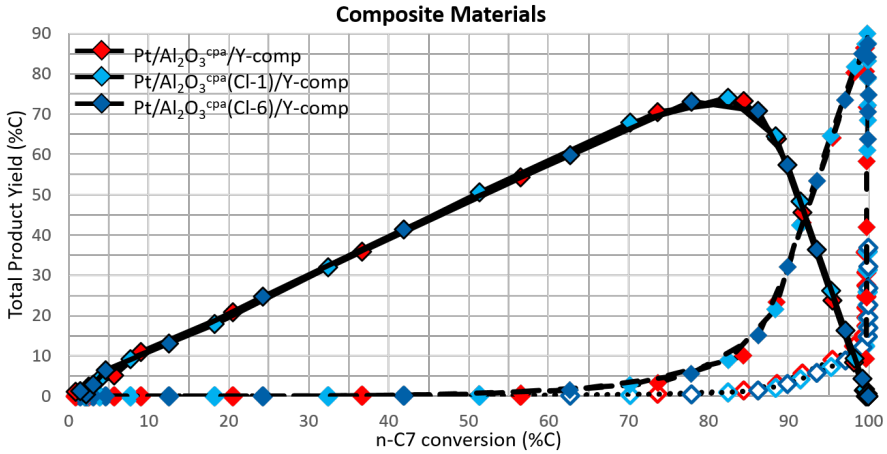

FIGURE 5.15: *Obtained product distribution in terms of isomerization (solid lines, filled/bordered symbols), primary cracking (dashed lines, filled symbols) and secondary cracking (dotted lines, open symbols) for the composite materials (light gray lines, rhombus symbols): $Pt/Al_2O_3^{cpa}$/Y-comp (red), $Pt/Al_2O_3^{cpa}$(Cl-1)/Y-comp (light blue) and $Pt/Al_2O_3^{cpa}$(Cl-6)/Y-comp (dark blue).*

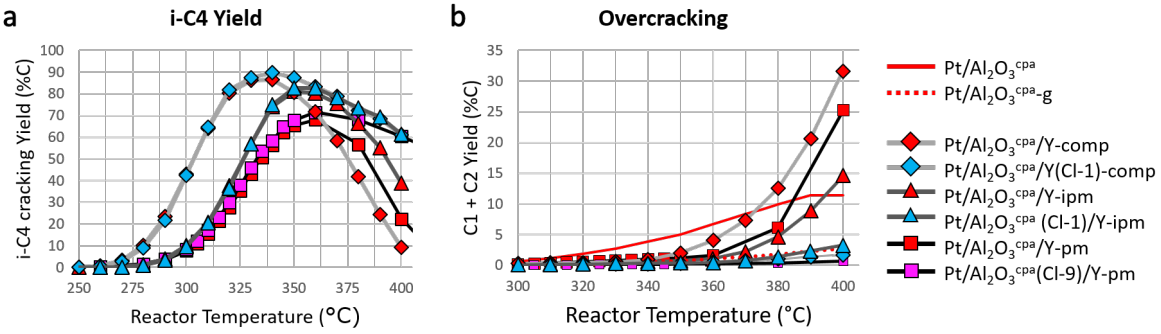

FIGURE 5.16: *a) Highlight of i-C4 cracking yield as function of reactor temperature of some bifunctional catalysts. b) Highlight of the amount of overcracking measured in (chlorine impregnated) bifunctional catalysts. A list of samples presented in 5.16 and is presented on the right.*

When the secondary cracking is studied in more detail, it is observed that chlorine impregnation quenches the formation of C1 and C2 hydrocarbons, which is presented in Figure 5.16b. Remarkably, in all intimacies and even in the reference samples it is observed that this overcracking is decreased to below 5% yield at chlorine impregnation concentrations as low as 1 wt.%. However, the same effect is seen when the average platinum nanoparticle size is increased with the growth protocol. For this reason, and considering the fact that only subtle differences in product distributions can be found as a result of chlorine impregnation in the bifunctional catalysts, this is most likely the result of platinum particle growth.

Because platinum is known to have considerable metal cracking activity, it was verified if this mechanism was contributing to the overall product selectivities in the zeolite based bifunctional catalysts. The product distribution arising from this mechanism, will mostly consist of linear hydrocarbons, and hence is quite comparable to product distribution of type C β-scission resulting from the bifunctional mechanism. There are only two products that can be formed by metal cracking but not by type C β-scission, which are n-hexane and methane as was shown in Figure 2.4 in Chapter 2. Considering that methane can also be formed as a result of overcracking or be formed by other mechanisms at higher temperatures, the formation of n-hexane is a more suitable indication to verify if metal cracking is occurring. It was observed that only the non zeolite containing reference samples had significant hexane yield. The zeolite based samples had a hexane yield of less than 1%. A highlight of this is given in Figure 5.17. It indicates that metal cracking only contributes to product distribution in the reference samples.

As a last analysis the activation energy of the n-heptane conversion was calculated for the catalysts. It was calculated that the composites had the lowest activation energy, around 120 kJ/mol. The intimate physical mixtures and physical mixtures had an Ea $\approx$ 150 kJ/mol and the Pt/Al_2O_3 catalysts had Ea $\approx$ 150 - 180 kJ/mol. As function of chlorine content, differences in the activation energy were calculated, although a clear trend was not observed. Results related to the calculation of the activation energy and corresponding Arrhenius plots are summarized in Appendix 9.7.

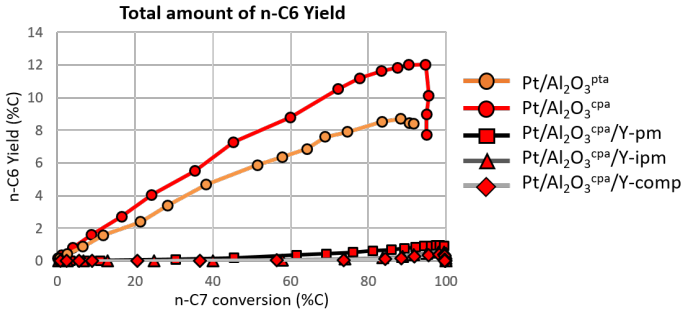

FIGURE 5.17: *Total yield of n-hexane as function of n-heptane conversion for $Pt/Al_2O_3^{pta}$ (orange circle/line), $Pt/Al_2O_3^{cpa}$ (red circle/line, $Pt/Al_2O_3^{cpa}$/Y-pm (red square/black line), $Pt/Al_2O_3^{cpa}$/Y-ipm (red triangle/dark gray line) and $Pt/Al_2O_3^{cpa}$/Y-comp (red rhombus/light gray line).*

Catalyst Stability

All zeolite based bifunctional catalyst were additionally tested at 360 °C. It was observed that the intimate physical mixtures and composite samples had less than 1% deactivation compared to the first measurement at 360°C. Furthermore, the deactivation of chlorine impregnated samples was comparable to the non chlorine impregnated bifunctional samples. However, in the case of the physical mixtures, significant deactivation was observed as function of chlorine content, even though all samples showed comparable initial n-heptane conversion of 88-89%. Already between $Pt/Al_2O_3^{pta}$/Y-pm and $Pt/Al_2O_3^{cpa}$/Y-pm, a difference in deactivation is observed, of which the latter shows 7% deactivation, while in the PTA prepared physical mixture no deactivation was observed. Upon chlorine impregnation the deactivation increases from 37% to 79% when going from $Pt/Al_2O_3^{cpa}$(Cl-9)/Y-pm to $Pt/Al_2O_3^{cpa}$(Cl-15)/Y-pm respectively, possibly indicating a chlorine dependence, which is presented in Figure 5.18.

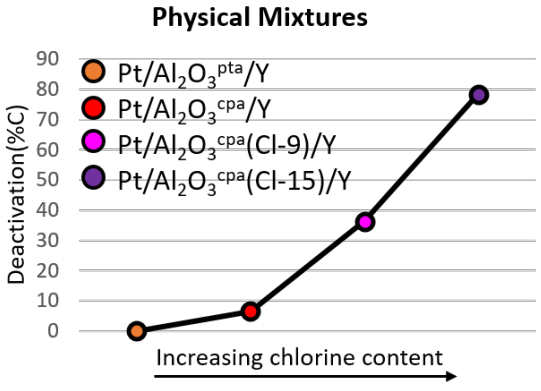

FIGURE 5.18: *Deactivation of physical mixtures, measured at 360°C, compared to initial conversion as function of introduced chlorine content.*

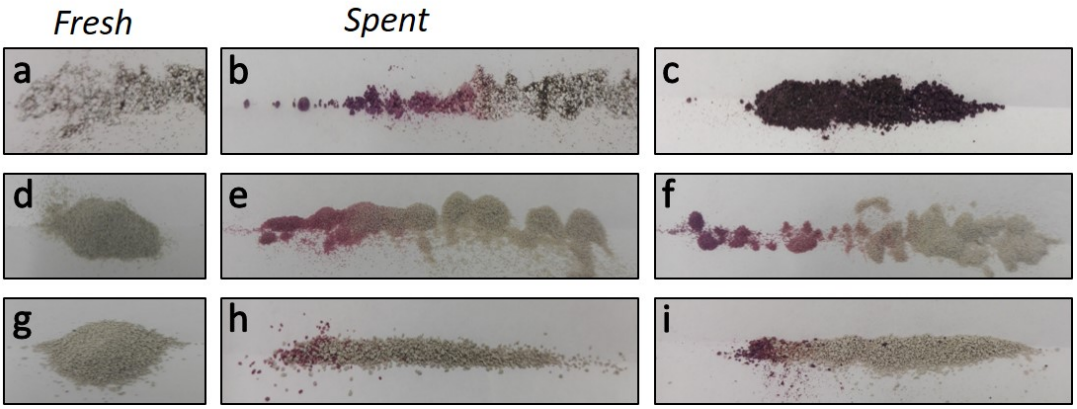

FIGURE 5.19: *Images of the spent catalysts compared to a fresh sample. a) fresh $Pt/Al_2O_3^{pta}$/Y-pm, b) spent $Pt/Al_2O_3^{pta}$/Y-pm, c) spent $Pt/Al_2O_3^{cpa}$(Cl-9)/Y-pm. Intimate physical mixtures: d) fresh $Pt/Al_2O_3^{pta}$/Y-ipm, e) spent $Pt/Al_2O_3^{pta}$/Y-ipm, f) spent $Pt/Al_2O_3^{cpa}$(Cl-6)/Y-ipm. Composites: g) fresh $Pt/Al_2O_3^{cpa}$/Y-comp, h) spent $Pt/Al_2O_3^{cpa}$/Y-comp, i) spent $Pt/Al_2O_3^{cpa}$(Cl-6)/Y-comp.*

When the zeolite based samples were compared to fresh catalysts, a remarkable observation was made. The spent catalysts were purple to pink on top. A highlight is shown in Figure 5.19. In the figure, the fixed bed reactors were emptied on the paper from left to right, so spent material positioned on the left was on top, while material on the right was at the bottom of the reactor. An increase in intimacy from millimeter scale to microscale seemed to result in formation of less purple material. Also, an increase in chlorine content, and thereby average platinum particle size, resulted in more purple material. However, since the highly intimate bifunctional catalysts showed no deactivation, this color change is most likely not directly related to that. As is shown in Figure 5.19c, the spent chlorine impregnated physical mixtures were very dark compared to a fresh sample, which is indicative of coke formation. Just as in the Pt/Al_2O_3 reference catalysts, this could be an indication of the fact that chlorine induced acid sites are not appropriate for bifunctional catalysis.

Chapter 6

Summary and Conclusions

From this study it can be concluded that not only is chlorine content challenging to remove, it is also challenging to quantify. ICP-OES results related to the chlorine content were shown to be more of a general indication rather than explicit. Furthermore, the influence of chlorine content on the surface acidity with NH_3-TPD yielded remarkably high NH_3 desorption values, most likely influenced by physisorption and platinum particle size, as was shown with a grown Pt/Al_2O_3 sample. Pyridine-IR results showed that $Pt/Al_2O_3{}^{cpa}$ and $Pt/Al_2O_3{}^{pta}$ had comparable signal with subtle distinctions, which were indicative of a slight difference in surface acidity. The analysis of the non zeolite based samples in terms of catalytic performance was complicated by the enhanced particle growth as a result of IWI with NH_4Cl. An increase of average platinum particle size resulted in decrease of total activity, a trend that was comparable to the chlorine impregnated samples. Also in the selectivity, overlap was observed. More isomerization and primary cracking yield were observed in both grown and chlorine impregnated Pt/Al_2O_3 catalyst.

In the catalytic performance results on the zeolite based bifunctional catalysts, it was presented that an increase in intimacy of the catalysts resulted in higher activity at lower reactor temperatures. The activity of the millimeter scale and microscale intimate catalysts, in which chlorine was introduced to the Pt/Al_2O_3 component, was only marginally affected by the addition. In the nanoscale intimate bifunctional catalysts, slight activity changes were visible as result of added chlorine content. These changes were most likely caused by the observed platinum relocation and growth on the zeolite component.

Also the selectivity of the conversion was influenced by the chlorine addition, although this difference became less prominent when the intimacy of the bifunctional catalysts was increased. Especially the physical mixtures were significantly influenced by the chlorine addition step and primary cracking yield increased as function of introduced chlorine content. In the nanoscale bifunctional catalysts, no distinction could be observed in selectivity as a result of the chlorine addition. Furthermore, the stability of the highly intimate bifunctional catalysts was not affected by the introduced chlorine content.

It can be concluded that chlorine content has a negligible effect on the catalytic performance of nanoscale bifunctional catalysts, hence a nanoscale intimacy is truly optimal for primary cracking yield.[15]

Chapter 7

Outlook

7.1 Measurement of Catalytic performance

In this study, the conversion of n-heptane has been applied as a model reaction for the hydrocarbon conversion. However, research has shown that other (longer) linear hydrocarbons can have significant effect on catalytic performance of bifunctional catalysts. When the isomerized product yield of bifunctional catalysts with ranging intimacies is compared with either a n-C10 or n-C19 feedstock, it is observed that the difference in catalytic performance is larger when a longer feedstock is applied.[15] Furthermore, a longer hydrocarbon feedstock can undergo type A β-scission and will be easier to crack. Therefore they might be more sensitive to smaller differences in catalyst acidity as a result of introduced chlorine content. However, a longer feedstock will complicate the analysis and isomer peaks will be more challenging to distinguish.

Significant deactivation variations were observed between the bifunctional catalysts, specifically the millimeter scale bifunctional catalysts. Although the highly intimate bifunctional catalysts showed only minimal deactivation, the observed color could indicate the formation of a non-active platinum species.

7.2 Sample Analysis

In this study sample analysis has been performed with NH_3-TPD and pyridine-IR. However, NMR studies might give more insight on the structure. With solid state Al-NMR the chemical surrounding of Al-atoms can be analyzed. In a study by Mirenko *et al.* on alumina samples, in which the effect of hydrothermal treatment temperature was considered, tetra, penta and octahedral oxygen environments around alumina atoms were observed at 70, 45 or 10 ppm respectively. Due to the high sensitivity of NMR analysis, ratios of these sites with respect to each other could be acquired.[66] Also, NMR in combination with basic probe molecules can give more insight in surface acidity. In general nitrogen based solid state NMR studies (^{15}N) give sensitivity problems in the data so they are challenging to analyze. However, phosphor based probe molecules (^{31}P) are attractive for studying surface acidity.[50] Handling TMP however, might be challenging as it reacts with air and can form explosive gases.[67]

The determination of chlorine content has been performed with ICP-OES, but in these data a wide variety was observed. Other techniques, reported in literature, like XPS,[60] titration,[52,59,68] XRF[55] or SEM-EDX[47,69] might be more appropriate for precise determination. Lastly, more pyridine-IR studies are necessary for more appropriate examination of Cl influence and data quantification.

Chapter 8

Acknowledgements

This thesis would not have been possible without the support and guidance of Jogchum Oenema. Thank you Jogchum, for your feedback, input and mentoring over the past year. I have really enjoyed my time on the thesis and have learned a great deal from you. I would also like express my gratitude towards prof. Krijn de Jong, for being my first examiner. Krijn, thank you for the fruitful discussions, kind words and enthusiasm. Further, I would like to acknowledge dr. Peter Ngene for being my second supervisor and valuable suggestions during the halfway meeting.

Additionally, I would like to thank Mark Meijerink, for the TEM/HAADF-STEM and EDX analysis, Ramon Oord for his help on the NH_3-TPD, Marjan Versluijs-Helder for the TGA-MS data and Suzanne Verkleij for her instructions on the pyridine-IR set-up. Also, a thank you to Lennart Weber and Tom van Deelen for their input and help on the Flowrence catalytic tests.

A special thanks to the ICC group, for the pleasant working atmosphere, which as a student alway made me feel welcome.

Chapter 9

Appendix

9.1 Temperature Profiles

The applied temperature profiles are schematically depicted in Figure 9.1a and b, for the reduction/aftertreatment and growth procedure respectively.

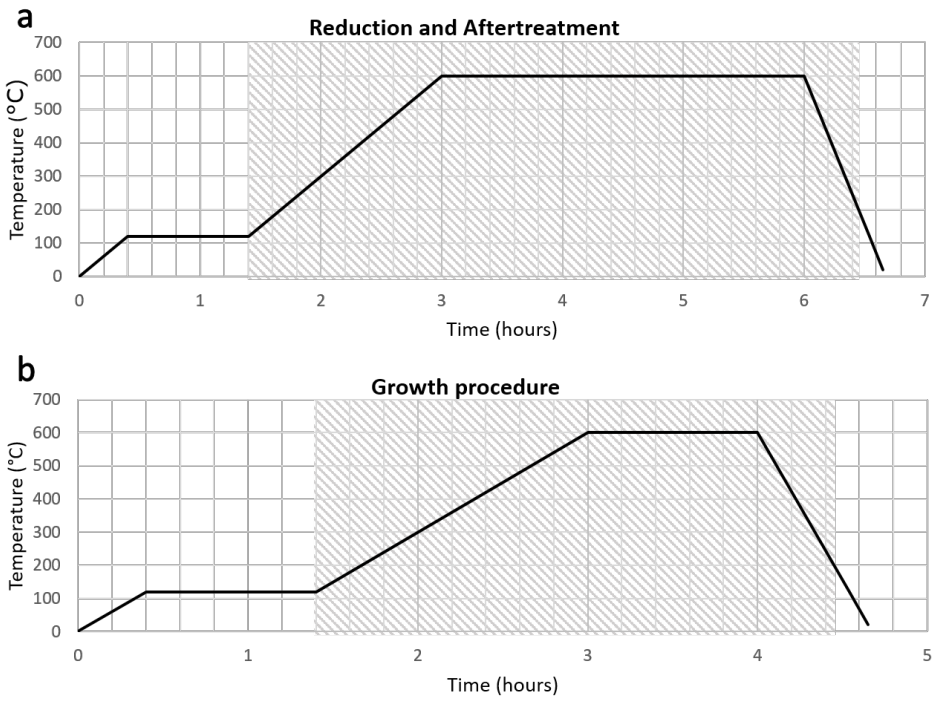

FIGURE 9.1: *Overview of temperature profiles applied for: 9.1a) The reduction and aftertreatment procedures. In the marked area, the atmosphere is changed from 100% N_2 to 100% H_2, with a flow of 100 mL/min/g catalyst. 9.1b) Growth procedure. In the marked area, the atmosphere is changed from 100% N_2 to 1 vol.% O_2 in N_2, with a flow of 100 mL/min/g catalyst. The heating ramps are 5°C/min. (cooling down at maximum ramp)*

9.2 Preparation of Pt/Al_2O_3 via SEA

Pt/Al_2O_3 has been prepared with both PTA and CPA precursor via SEA.

The preparation of $Pt/Al_2O_3{}^{cpa}$-sea, occurred without obstacles and a Pt weight loading around 1 wt.% was readily achieved. The preparation of $Pt/Al_2O_3{}^{pta}$-sea on the other hand, proved challenging. These samples contained insufficient weight loading of Pt around 0.1 wt.%, which was likely caused by the solvent pH. pH=11.5, the optimal pH for adsorption of PTA on a γ-alumina surface as was shown in Figure 2.6, is challenging to achieve with a weak base like ammonia. Therefore, a 1M NaOH solution was also applied to prepare $Pt/Al_2O_3{}^{pta}$-sea. Even though pH=11.5 was easily achieved with this strong base, the SEA procedure was ineffective for increasing the platinum weight loading.

The preparation of Pt/Al_2O_3 via SEA was performed with a γ-alumina prepared from a 70 wt.% Boehmite. ICP-OES analysis of only support material revealed that the obtained γ-alumina contained a significant amount of chlorine content. For this reason, samples prepared via IWI have been prepared with an extra pure γ-alumina puralox-SCCa variant.

9.3 Additional TEM results

Obtained HAADF-STEM results and corresponding size distributions of Pt/SiO_2^{pta}, $Pt/Al_2O_3^{pta}$-g and $Pt/Al_2O_3^{cpa}$-g are presented in Figure 9.2a, b and c respectively.

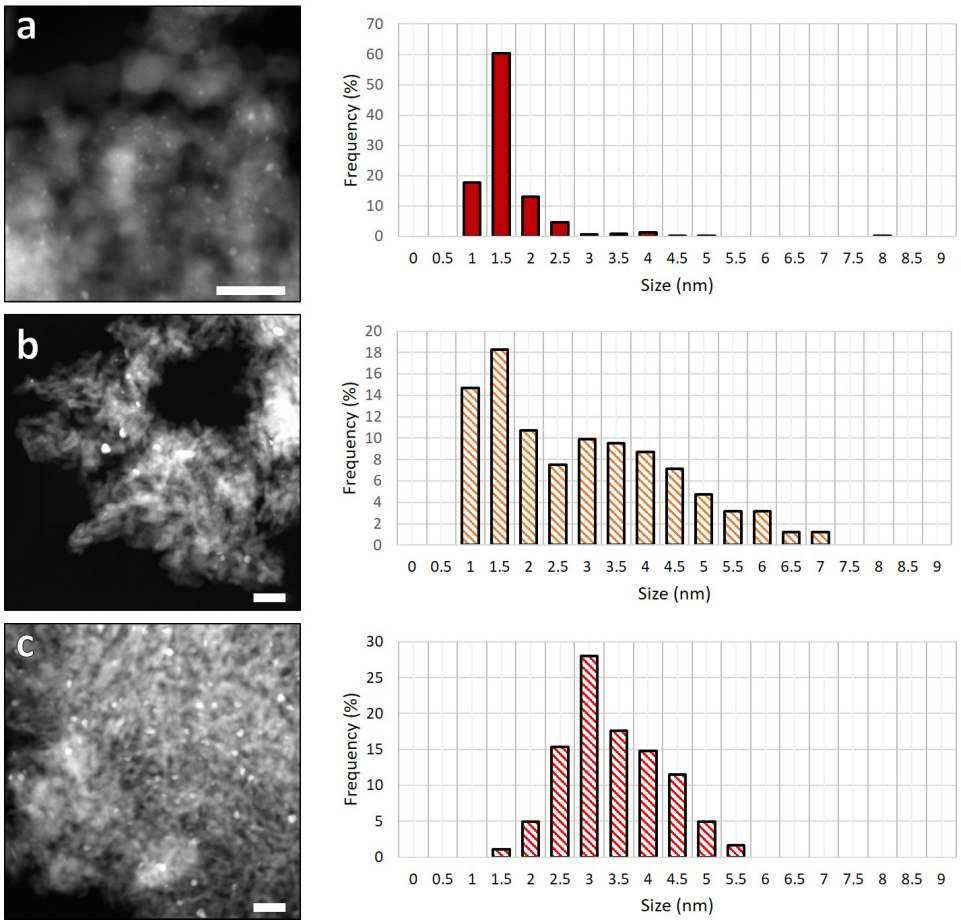

FIGURE 9.2: *Overview of HAADF-STEM results on a) Pt/SiO_2^{pta}, b) $Pt/Al_2O_3^{pta}$-g and c) $Pt/Al_2O_3^{cpa}$-g. Scale bars are 20 nm.*

9.4 Additional TGA-MS results on $Pt/Al_2O_3(Cl)$

The detailed TGA-MS results on the non aftertreated $Pt/Al_2O_3(Cl)$, which was impregnated with a saturated NH_4Cl solution is depicted in Figure 9.3. No clear peaks in MS signals were observed that could be correlated to the measured weight decrease of the sample.

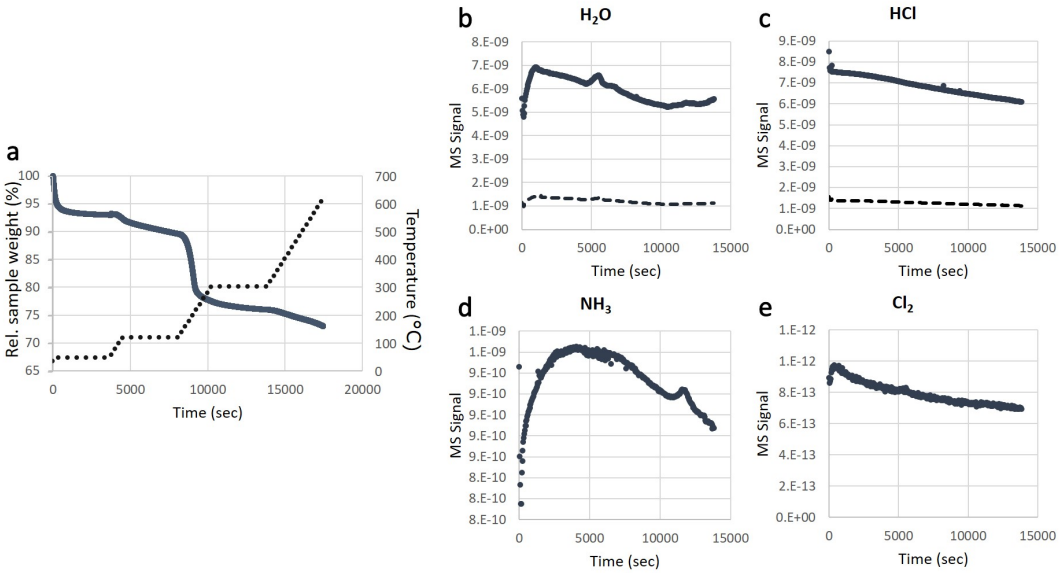

FIGURE 9.3: *a) relative sample weight (blue) and reactor temperature (black/dotted) as function of time. b) MS data of 18 (solid) m/z, and 17 (dashed) m/z, corresponding to H_2O. c) MS data of 36 (solid) m/z and 38 (dashed) m/z, corresponding to HCl. d) MS data of 16 (solid) m/z, corresponding to NH_3. e) MS data of 70 (solid) m/z, corresponding to Cl_2.*

9.5 NH_3-TPD data

In Figure 9.4, the TCD signal of the double impregnated samples as function of temperature are depicted. The deconvoluted plots which were applied for calculation of ammonia desorption are shown in Figure 9.5.

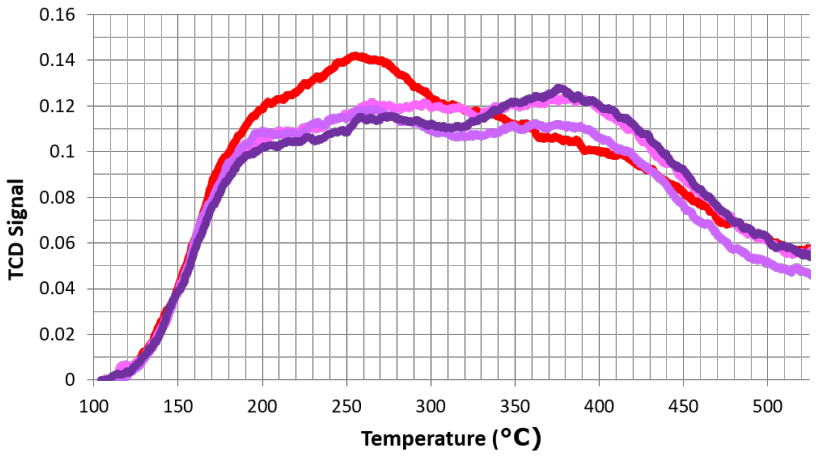

FIGURE 9.4: *NH_3-TPD results for all double impregnated samples compared to $Pt/Al_2O_3{}^{cpa}$ (red): $Pt/Al_2O_3{}^{cpa}$(Cl-9) (pink), $Pt/Al_2O_3{}^{cpa}$(Cl-12) (light purple) and $Pt/Al_2O_3{}^{cpa}$(Cl-15) (dark purple).*

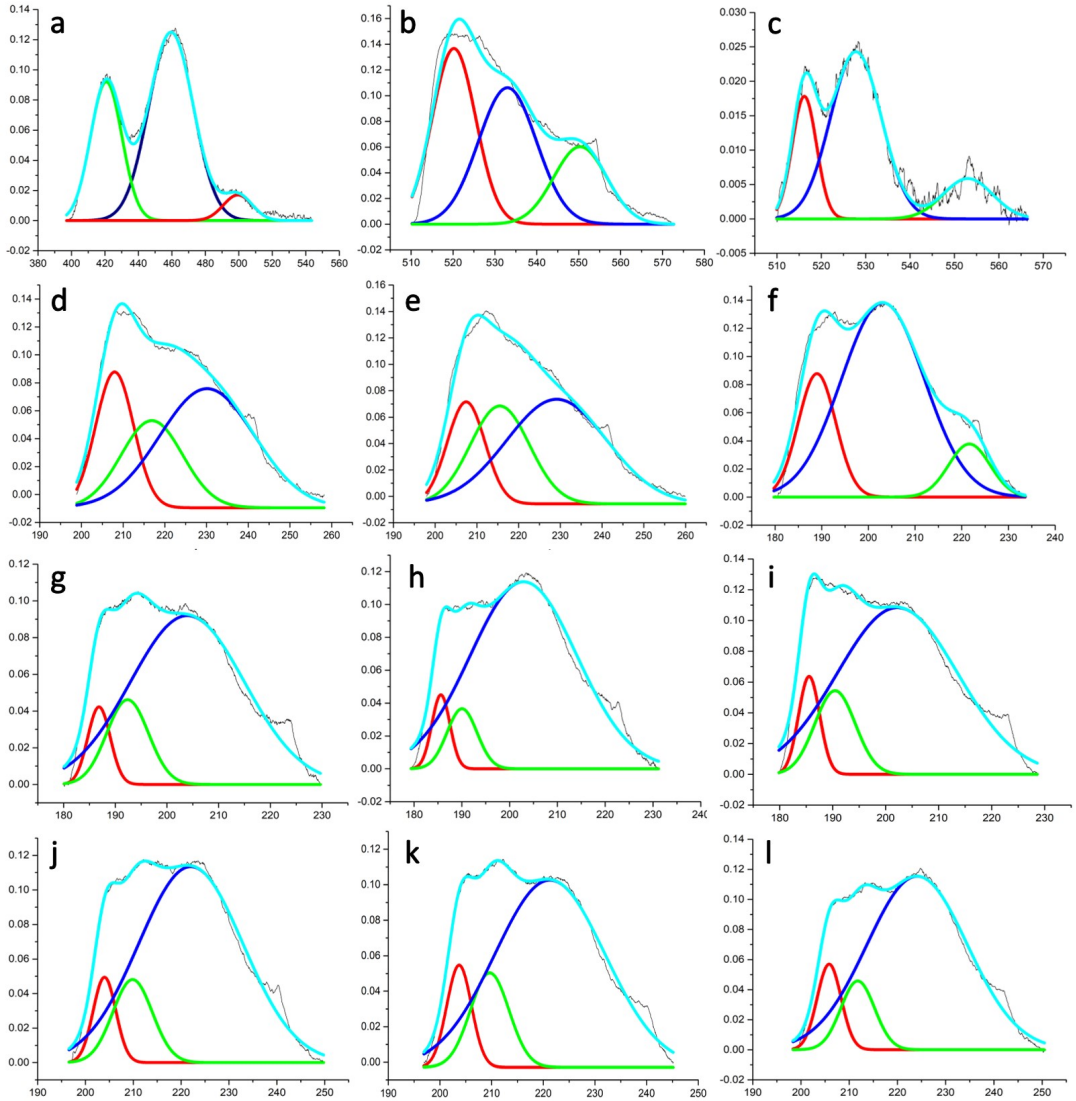

FIGURE 9.5: *TCD signal vs. time (min) plots and corresponding deconvolution. Dark blue areas are taken as strong acid site signal. Light blue areas are applied for total NH_3 desorption calculation. a) CBV760 b) γ-alumina, c) Pt/SiO_2^{pta}, d) $Pt/Al_2O_3^{pta}$, e) $Pt/Al_2O_3^{cpa}$, f) $Pt/Al_2O_3^{cpa}$-g, g) $Pt/Al_2O_3^{cpa}$(Cl-1), h) $Pt/Al_2O_3^{cpa}$(Cl-3), i) $Pt/Al_2O_3^{cpa}$(Cl-6), j) $Pt/Al_2O_3^{cpa}$(Cl-9), k) $Pt/Al_2O_3^{cpa}$(Cl-12), l) $Pt/Al_2O_3^{cpa}$(Cl-15).*

9.6 TOF calculation results

The TOF of metal cracking in the reference samples has been calculated per mol of surface platinum, as shown in Formula 9.1. The total amount of Pt surface has been calculated with formulas 9.2, 9.3 and 9.4.

$$TOF(s^{-1}) = F * Mc * Pt^{surf.} \tag{9.1}$$

$$Pt^{surf.} = Pt^{mol} * Pt^{disp.} \tag{9.2}$$

$$Pt^{mol} = Pt\% * m * Pt^{molM.} \tag{9.3}$$

$$Pt^{disp.} = \frac{1}{\sum d^3 / \sum d^2} \tag{9.4}$$

- F = Flow of n-C7 (mol/s)
- Mc = Metal cracking yield as described in experimental.
- $Pt^{surf.}$ = Amount of surface platinum (mol).
- Pt^{mol} = Moles of platinum in the catalyst.
- $Pt^{disp.}$ = Platinum dispersion.
- Pt% = Platinum wt.% in the samples, according to (average) ICP-OES.
- m = Mass of catalysts loaded in the fixed bed reactor (g).
- $Pt^{molM.}$ = Molar mass of platinum (195.078 g/mol).
- d = Nanoparticle diameter (per particle), measured with HAADF-STEM (nm).

Figure 9.6 presents the obtained results, including the calculated platinum dispersions. Several observations are made. First of all, increasing the platinum particle size of Pt/Al_2O_3 results in an increase in metal cracking TOF for non chlorine impregnated samples, of which $Pt/Al_2O_3^{pta}$-g shows the highest increase compared to $Pt/Al_2O_3^{cpa}$-g. In the chlorine containing samples, a higher introduced content (and with that a decreased platinum dispersion) lowers the metal cracking TOF. Furthermore, Pt/SiO_2^{pta} shows a significantly higher TOF than the non grown Pt/Al_2O_3, even though the sample contains a lower dispersion. However, at temperatures below 350 °C, the obtained TOF for all Pt/Al_2O_3 catalysts are comparable.

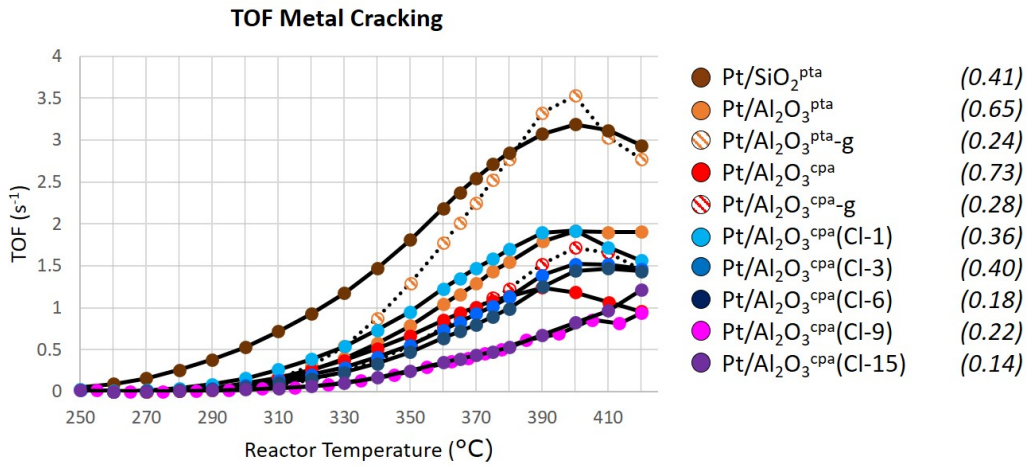

FIGURE 9.6: *Metal Cracking turn over frequency (s^{-1}) for the reference catalysts. Calculated platinum dispersions are depicted in brackets.*

9.7 Calculation of Ea

The activation energy for the conversion of n-heptane was calculated for the Pt/Al_2O_3 references and zeolite based bifunctional catalysts, via the Arrhenius equation, depicted in Formula 9.5. When $ln(k)$ is plotted as function of $\frac{1}{T}$, multiplication of the slope by the gas constant R will yield Ea. k is calculated via Formula 9.6. In this calculation, first order kinetics in a plug flow reactor are assumed. The conversion, χ_a, is defined as a value between '0' and '1' and is therefore calculated out of the measured conversion (%C) via Formula 9.7. The residence time τ, defined as the reciprocal of the weight hourly space velocity (WHSV), is calculated via Formula 9.8.[70]

$$ln(k) = ln(A) - \frac{Ea}{R} * \frac{1}{T} \tag{9.5}$$

$$k = -\frac{ln(1-\chi_a)}{\tau} \tag{9.6}$$

$$\chi_a = \frac{C7_{Conv.}}{100} \tag{9.7}$$

$$\tau = \frac{1}{WHSV} * \frac{1}{3600} \tag{9.8}$$

- k = First order rate constant (s^{-1}).
- A = Pre-exponential factor (unitless).
- Ea = Activation energy (J/mol).
- R = Gas constant (8.314 J/mol/K).
- T = Reaction temperature (K).
- χ_a = Conversion (mol/mol).
- τ = Residence time (s).
- $C7_{Conv.}$ = Conversion as measured in catalytic test (%C).
- WHSV = Weight hourly space velocity (h^{-1}).

A highlight of the obtained Arrhenius plots is given in Figure 9.7. It is observed in the plots that a clear separation is present between the reference samples and the ranging intimacies. The calculated activation energies are summarized in Tables 9.1 and 9.2. The non chlorine impregnated Pt/Al_2O_3 references all have an activation energy around 180 kJ/mol. Upon Cl introduction, this energy decreases, although a clear trend is not observed. In the zeolite based bifunctional catalysts, an increase in intimacy results in a decrease of activation energy. Furthermore, increase in chlorine content in the nanoscale bifunctional catalysts results in an enhanced Ea up to 135 kJ/mol. In the physical mixtures and intimate physical mixtures, this Cl introduction does not lead to significant changes in activation energy. The calculated activation energies for the zeolite containing samples are comparable to a study by Kinger *et al.* in which the activation energy for platinum containing mixtures of zeolites with inert materials was calculated.[32]

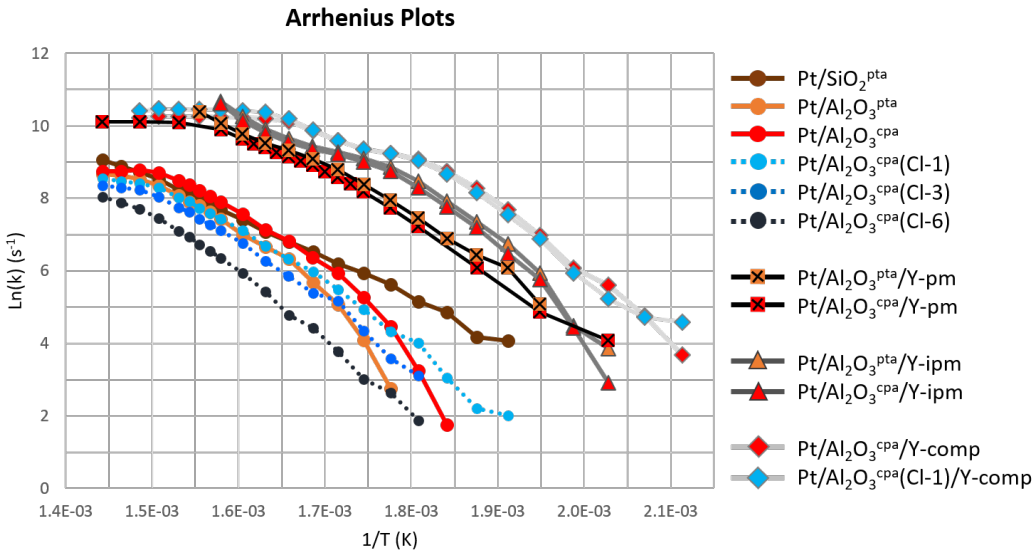

FIGURE 9.7: *Highlight of Arrhenius plots, calculated via depicted formulas. A legend is shown on the right.*

Sample name	Ea (kJ/mol)
Pt/SiO_2^{pta}	90
$Pt/Al_2O_3^{pta}$	188
$Pt/Al_2O_3^{pta}$-g	183
$Pt/Al_2O_3^{cpa}$	183
$Pt/Al_2O_3^{cpa}$-g	182
$Pt/Al_2O_3^{cpa}$(Cl-1)	126
$Pt/Al_2O_3^{cpa}$(Cl-3)	149
$Pt/Al_2O_3^{cpa}$(Cl-6)	167
$Pt/Al_2O_3^{cpa}$(Cl-9)	120
$Pt/Al_2O_3^{cpa}$(Cl-12)	164
$Pt/Al_2O_3^{cpa}$(Cl-15)	150

TABLE 9.1

Sample name	Ea (kJ/mol)
$Pt/Al_2O_3^{pta}$/Y-pm	141
$Pt/Al_2O_3^{cpa}$/Y-pm	135
$Pt/Al_2O_3^{cpa}$(Cl-9)/Y-pm	128
$Pt/Al_2O_3^{cpa}$(Cl-15)/Y-pm	136
$Pt/Al_2O_3^{pta}$/Y-ipm	139
$Pt/Al_2O_3^{cpa}$/Y-ipm	146
$Pt/Al_2O_3^{cpa}$(Cl-1)/Y-ipm	147
$Pt/Al_2O_3^{cpa}$(Cl-3)/Y-ipm	144
$Pt/Al_2O_3^{cpa}$(Cl-6)/Y-ipm	138
$Pt/Al_2O_3^{cpa}$(Cl-9)/Y-ipm	139
$Pt/Al_2O_3^{cpa}$/Y-comp	112
$Pt/Al_2O_3^{cpa}$(Cl-1)/Y-comp	120
$Pt/Al_2O_3^{cpa}$(Cl-6)/Y-comp	135

TABLE 9.2

Overview of the calculated activation energies. 9.1: Ea of the Pt/Al_2O_3 reference samples. The slope is calculated between 300 and 340 °C. 9.2: Ea of the zeolite based bifunctional catalysts. The slope is calculated between 240 and 290 °C.

Bibliography

(1) Chorkendorff, I.; Niemantsverdriet, J., *Concepts of Modern Catalysis and Kinetics*, 1st ed.; Wiley VCH: 2003.

(2) Thomas, J.; Harris, K. *Energ. Environm. Sci.* **2016**, *9*, 687–708.

(3) Staff 'Report petrochemical market'., www.processingmagazine.com/petrochemical-market-worth-758-3-billion-2022, Accessed: 2018-01-04.

(4) Hagen, J., *Industrial Catalysis*, 3rd ed.; Wiley VCH: 2015, pp 299–317.

(5) Sadeghbeigi, R., *Fluid catalytic cracking handbook: an expert guide to the practical operation, design, and optimization of FCC units*, 1st ed.; Butterworth-Heinemann: 2012.

(6) Rana, M.; Sámano, V.; Ancheyta, J.; Diaz, J. *Fuel* **2006**, *86*, 1216–1231.

(7) Bruice, P., *Organic Chemistry*, 7th ed.; Pearson: 2014, pp 101–104.

(8) Smolenskii, E.; Bavykin, V.; Ryzhov, A.; Slovokhotova, O.; Chuvaeva, I.; Lapidus, A. *Russ. Chem. B.* **2008**, *57*, 461–467.

(9) Somorjai, G. *J. Catal.* **1972**, *27*, 453–456.

(10) Marint, G.; Froment, G. *Chem. Eng. Sci.* **1982**, *5*, 759–773.

(11) Huber, G.; Iborra, S.; Corma, A. *Chem. Rev.* **2006**, *106*, 4044–4098.

(12) Mata, T.; Martins, A.; Martins; Caetano, N. *Renew. Sust. Energ. Rev.* **2010**, *14*, 217–232.

(13) Jahangiri, H.; Bennet, J.; Mahjoubi, P.; Wilson, K.; Gu, S. *Catal. Sci. Technol.* **2014**, *4*, 2210–2229.

(14) Thybaut, J.; Marin, G. *Adv. Catal.* **2016**, *59*, 109–238.

(15) Zečević, J.; Vanbutsele, G; de Jong, K.; Martens, J. *Nature* **2015**, *528*, 245–248.

(16) Regali, F.; Liotta, L.; Venezia, A.; Boutonnet, M.; Järås, S. *Appl. Catal. A Gen.* **2014**, *469*, 328–339.

(17) Kenmogne, R.; Finiels, A.; Cammarano, C.; Hulea, V.; Fajula, F. *J. Catal.* **2015**, *329*, 348–354.

(18) Alvarez, F.; Ribeiro, F.; Perot, G.; Thomazeau, C.; Guisnet, M. *J. Catal.* **1996**, *162*, 179–189.

(19) Guisnet, M. *Catal. Today* **2013**, *218-219*, 123–134.

(20) Toulhoat, H.; Raybaud, P.; Benazzi, E. *J. Catal.* **2004**, *221*, 500–509.

(21) Benazzi, E.; Leite, L.; Marchal-George, N.; Toulhoat, H.; Raybaud, P. *J. Catal.* **2003**, *217*, 376–387.

(22) Batalha, N.; Pinard, L.; Pouilloux, Y.; Guisnet, M. *Catal. Lett.* **2013**, *143*, 587–591.

(23) Batalha, N.; Pinard, L.; Bouchy, C.; Guillon, E.; Guisnet, M. *J. Catal.* **2013**, *307*, 122–131.

(24) Samad, J.; Blanchard, J.; Sayag, C.; Louis, C.; Regalbuto, J. *J. Catal.* **2016**, *342*, 203–212.

(25) Weisz, P. *Adv. Catal.* **1962**, *13*, 137–190.

(26) Deutschmann, O., *Heterogeneous Catalysis and Solid Catalysts*, 2nd ed.; Wiley-VCH: Weinheim, 2009.

(27) Paulis, M.; Peyrard, E.; Montes, M. *J. Catal.* **2001**, *199*, 30–40.

(28) Jain, A.; Pradhan, N.; Dalai, A.; Bakhshi, N. *Catal. Lett.* **2003**, *86*, 221–227.

(29) Weitkamp, J. *ChemCatChem* **2012**, *4*, 292–306.

(30) Kim, J.; Kim, W.; Seo, Y.; Kim, J.; Ryoo, R. *J. Catal.* **2013**, *301*, 187–197.

(31) Ono, Y. *Catal. Today* **2003**, *81*, 3–16.

(32) Kinger, G.; Majda, D.; Vinek, H. *Appl. Catal. A Gen.* **2002**, *225*, 301–312.

(33) Coonradt, H.; Garwood, W. *Ind. Eng. Chem. Proc. DD.* **1964**, *3*, 38–45.

(34) Wang, Y.; Tao, Z.; Wu, B.; Xu, J.; Huo, C.; Li, K.; Chen, H.; Yang, Y.; Li, Y. *J. Catal.* **2015**, *322*, 1–13.

(35) Kotrel, S.; Knözinger, H.; Gates, B. *Micropor. Mesopor. Mat.* **2000**, *35*, 11–20.

(36) Carter, J.; Cusumano, J.; Sinfelt, J. *J. Catal.* **1971**, *20*, 223–229.

(37) Carvalho, L.; Reyes, P.; Pecchi, G.; Figoli, N.; Pieck, C.; Do, M.; Rangel, C. *Ind. Eng. Chem. Res.* **2001**, *40*, 5557–5563.

(38) Boubnov, A.; Dahl, S.; Johnson, E.; Molina, A.; Simonsen, S.; Cano, F.; Lemus-Yegres, L.; Grunwaldt, J. *Appl. Catal. B Environ.* **2012**, *126*, 315–325.

(39) de Graaf, J.; van Dillen, A.; de Jong, K.; Koningsberger, D. *J. Catal.* **2001**, *203*, 307–321.

(40) Liu, Q.; Joshi, U.; Über, K.; Regalbuto, J. *Phys. Chem. Chem. Phys.* **2014**, *16*, 26431–26435.

(41) Augustine, S.; Alameddin, G.; Sachtler, W. *J. Catal.* **1989**, *115*, 217–232.

(42) Burnens, G.; Bouchy, C.; Guillon, E.; Martens, J. *J. Catal.* **2011**, *282*, 145–154.

(43) Spieker, W.; Regalbuto, J. *Chem. Eng. Sci.* **2001**, *56*, 3491–3504.

(44) Brunelle, J. *Pure Appl. Chem.* **1978**, *50*, 1211–1229.

(45) Batalha, N.; Pinard, L.; Morisset, S.; Lemberton, J.; Pouilloux, Y.; Guisnet, M.; Lemos, F.; Ribeiro, F. *React. Kinet. Mech. Catal.* **2012**, *107*, 285–294.

(46) Mendes, P.; Mota, F.; Silva, J.; Ribeiro, M.; Daudin, A.; Bouchy, C. *Catal. Sci. Technol.* **2014**, *7*, 1095–1107.

(47) Ito, K.; Ohshima, M.; Kurokawa, H.; Sugiyama, K.; Miura, H. *Catal. Commun.* **2002**, *3*, 527–531.

(48) Castro, A.; Scelza, O.; Benvenuto, E.; Baronetti, G.; Parera, J. Regulation of the chlorine content on Pt/Al2O3 catalyst., 1981.

(49) Atkins, P.; Overton, T.; Rourke, J.; Weller, M.; Armstrong, F., *Inorganic Chemistry*, 5th ed.; Oxford University Press: 2010, pp 111–144.

(50) Guillaume, D.; Gautier, S.; Alario, F.; Devès, J. *Oil Gas Sci. Technol.* **1999**, *54*, 537–545.

(51) Liu, J.; Liu, C.; Ma, A.; Rong, J.; Da, Z.; Zheng, A.; Qin, L. *Appl. Surf. Sci.* **2016**, *368*, 233–240.

(52) Jain, A.; Pradhan, N.; Dalai, A.; Bakhshi, N. *Catal. Lett.* **2003**, *86*, 221–227.

(53) Tanaka, M.; Ogasawara, S. *J. Catal.* **1970**, *16*, 157–163.

(54) Beard, B.; Zhang, Z. *Catal. Lett.* **2002**, *82*, 1–5.

(55) Digne, M.; Raybaud, P.; Sautet, P.; Guillaume, D.; Toulhoat, H. *J. Am. Chem. Soc.* **2008**, *130*, 11030–11039.

(56) Nortier, P.; Fourre, P.; Saad, A.; O., S.; Lavalley, J. *Appl. Catal.* **1990**, *61*, 141–160.

(57) Bernard, P.; Primet, M. *J. Chem. Soc.* **1990**, *86*, 567–570.

(58) Melchor, A.; Garbowski, E.; Mathieu, M.; Primet, M. *J. Chem. Soc.* **1986**, *82*, 1893–1901.

(59) Figoll, N.; Sad, M.; Bekramlnl, J.; Jablonskl, E.; Parera, J. *Ind. Eng. Chem. Prod. Res. Dev* **1980**, *19*, 545–551.

(60) Mazzieri, V.; L'Argentière, P.; Coloma-Pascual, F.; Fígoli, N. *Ind. Eng. Chem. Res.* **2003**, *42*, 2269–272.

(61) Liu, Q.; Samad, J.; Copple, J.; Eskandari, S.; Satterwhite, C.; Regalbuto, J. *Catal. Today* **2017**, *280*, 246–252.

(62) Lee, H.; Kim, W.; Jung, K.; Koh, H. *Korean J. Chem. Eng.* **2017**, *34*, 1337–1345.

(63) Hoang, D.; Farrage, S.; Radnik, J.; Pohl, M.; Schneider, M.; Lieske, H.; Martin, A. *Appl. Catal. A. Gen.* **2007**, *333*, 67–77.

(64) Knözinger, H., *Infrared Spectroscopy for the Characterization of Surface Acidity and Basicity*, 1st ed.; Wiley VCH: 2008, pp 1135–1163.

(65) Vimont, A. *presentation slides: IR probe molecules for acidic sites* **2016**.

(66) Mironenko, R.; Belskaya, O.; Talsi, V.; Gulyaeva, T.; Kazakov, M.; Nizovskii, A.; Kalinkin, A.; Bukhtiyarov, V.; Lavrenov, A.; Likholobov, V. *Appl. Catal. A Gen.* **2014**, *469*, 472–482.

(67) Sigma-Aldrich 'Material Safety Data Sheet of TMP'., www.sigmaaldrich.com/catalog/substance/trimethylphosphate1400751256111, Accessed: 2018-01-11.

(68) Marceau, E.; Che, M.; Saint-Just, J.; Tatibouet, J. *Catal. Today* **1996**, *29*, 415–419.

(69) Liu, Z.; Xiao-Hong, L.; Zhi-Jian, C.; Pinliang, Y.; Zhao-Chi, F.; Can, L. *J. Fuel Chem. Techn.* **2009**, *37*, 205–211.

(70) Hanefeld, U.; Lefferts, L., *Catalysis*, 1st ed.; Wiley VCH: 2018, pp 211–270.